LEVEL

12

AD A102267

NAVAL AIR PROPULSION CENTER

TRENTON, NEW JERSEY 08628

NAPC-PE-33 JANUARY 1981
NASA-CR-165389

ROTOR FRAGMENT PROTECTION PROGRAM: EXPERIMENTATION TO PROVIDE GUIDELINES FOR THE DESIGN OF TURBINE ROTOR FRAGMENT CONTAINMENT RINGS

By J. T. SALVINO & R. A. DeLUCIA

APPROVED FOR PUBLIC RELEASE: DISTRIBUTION UNLIMITED

NAVAL AIR PROPULSION CENTER

TRENTON, NEW JERSEY 08628

PROPULSION TECHNOLOGY AND PROJECT ENGINEERING DEPARTMENT

NAPC-PE-33 JANUARY 1980
NASA-CR-165389

ROTOR FRAGMENT PROTECTION PROGRAM: EXPERIMENTATION TO PROVIDE GUIDELINES FOR THE DESIGN OF TURBINE ROTOR FRAGMENT CONTAINMENT RINGS

Prepared by: J. T. Salvino
J. T. SALVINO

R. A. DeLucia
R. A. DeLUCIA

Approved by: J. L. Moss
J. L. MOSS
Commander, USN
Director, PE

APPROVED FOR PUBLIC RELEASE:
DISTRIBUTION UNLIMITED

AUTHORIZATION: NASA DPR C-41581-B, MOD. 10

FOREWORD

This report has been prepared by the Naval Air Propulsion Center, Trenton, New Jersey under NASA Defense Purchase Request C-41581-B Modification No. 10 from the Lewis Research Center, National Aeronautics and Space Administration, Cleveland, OH 44135. Mr. Solomon Weiss, and Dr. Arthur Holms of the Lewis Research Center served as program monitors. Their contributions and help during this program are greatly appreciated. The authors would like to thank Dr. Emmett A. Witmer, Dr. John W. Leech, Mr. R. P. Yeghiayan, Mr. F. Merlis, and Mr. T. R. Stagliano, Massachusetts Institute of Technology, for their conceptual and analytical support and consultation.

TABLE OF CONTENTS

LIST OF FIGURES

SUMMARY

The program of parametric rotor fragment containment experimentation being reported was developed and conducted by the Naval Air Propulsion Center (NAPC) under National Aeronautics and Space Administration (NASA) sponsorship. The program objective is to develop guidelines for the design of optimum weight containment rings for turbine engine rotor fragments.

Rotor/disk and blade containment experiments were conducted using strain gage instrumented containment rings. The tests were conducted to study, by means of high-speed photography and strain measurements, the interaction that takes place between the rotor fragments and containment ring during the containment process. The recorded information was supplied to the Aeroelastic Structures Research Laboratory of the Massachusetts Institute of Technology for use in the TEJ-2 or CIVM JET-4B computer programs which are being developed for use in the optimum design of containment/deflection devices.

The characterization of blade and rotor fragment behavior and containment ring response was made possible by photographing blades and rotors intentionally modified to fail at their design operating speed.

INTRODUCTION

The Rotor Fragment Protection Program (RFPP) is sponsored by the National Aeronautics and Space Administration (NASA) and conducted by the Naval Air Propulsion Center (NAPC) in conjunction with the Massachusetts Institute of Technology (MIT). The objective of the program is to develop guidelines for the design of light weight devices that will protect aircraft and their passengers from fragments generated by failed gas turbine engine rotating components.

Previous reports published by the NAPC, which document the progress of this program and present parametric test results, are listed as references 1, 2, 3, 4, 5, and 6.

This report presents the results of experiments conducted by the NAPC on instrumented containment rings in order to obtain displacement and strain information during fragment/containment ring interaction. The experiments were conducted to assist MIT in their research efforts to analytically predict the permanent deflection and the elastic-plastic transient responses of containment devices upon fragment impact. The strain data and high speed film obtained from the experiments conducted in the Rotor Spin Facility of the NAPC were supplied to the Aeroelastic and Structures Research Laboratory (ASRL) of MIT.

The containment ring transient and permanent strains recorded from test 201 and presented in this report are considered to be typical of the strains and responses that could be expected when the containment ring succeeds in containing the fragments.

CONCLUSIONS

1. Through the use of high-speed photography, a successful characterization of fragment behavior and containment ring response during a typical 3-fragment containment event can be made.

2. Gross deformation of the ring begins after the blades have deformed and the undeformable disk sector impacts the ring. The blades therefore cause very little deformation of the ring.

OBJECTIVE

The blade and rotor fratment containment tests were conducted to:

Study the blade/rotor and ring interactions and deformations during the containment process.

Record (by high-speed photography) and measure the ring displacements with respect to time.

Record and measure the transient and permanent strains encountered by the containment rings during and as a result of this containment process.

Provide MIT with the recorded data for use in their TEJ-2 (references 7 and 8) and CIVM JET-4B (reference 9) computer programs, which estimate the force-time characteristics of ring and fragments during the containment process.

METHOD OF TEST

The test results presented in this report were obtained using basically the same equipment and techniques described in references 3 and 4. Figure 1 shows a typical setup. Basically, the test procedure is as follows:

The test rotor, modified to fail and produce particular shaped fragments at a specified speed, is connected to the air-drive turbine by an arbor. The containment ring under test is freely suspended by guidewires and is concentrically positioned around the test rotor. The axial mid section of the ring is positioned to coincide with test rotor's plane of rotation. The photo-triggering strip is fixed to the inner diameter of the containment ring in the rotor plane of rotation and is connected to the flash circuitry. A photographic mirror (front surface) is positioned at a 45 degree angle to the optical axis of the high-speed camera for full plane action coverage beneath the rotor. The spin chamber is evacuated to 10 mm Hg pressure in order to reduce the aerodynamic drag on the test rotor and thus the power required to accelerate the rotor to its failure speed. In order to record the fragment/containment ring interactions on film: the spin chamber is completely dark; the rotating drum type camera is accelerated to the desired framing rate with the camera capping shutter open; the test rotor or fragment generator is accelerated to the desired failure speed; when the fragment is released and makes contact with the inner surface of the containment ring, the trigger circuit is activated which flashes the lights thus capturing the event on film.

The containment rings were instrumented with strain gages to measure the transient and permanent strains produced by fragment impact. The gages were attached to the ring at various circumferential locations on the ring axial center line using M-bond AE-15 adhesive (see Appendix A-9).

DESCRIPTION OF EXPLORATORY EXPERIMENTS

Table I lists the rotor/disk and blade containment experiments that were conducted with instrumented containment rings; it also describes the materials used and conditions of each experiment. The experiments were conducted to characterize the containment ring dynamics and deformations involved in the containment of blade and rotor fragments at failure.

In the rotor fragment containment experiments, GE-T58 engine power turbine rotors (full-bladed) were modified to fail at design operating speed into three equal pie-shaped fragments and impact instrumented containment rings which were centrifugally cast from 4130 steel.

In the blade fragment containment experiments, blades from GE-T58 engine power turbine rotors were modified to fail at design speed and impact instrumented containment rings made from 6061 (T6) and 2024 (T4) aluminum. These ring materials were selected because of their well known mechanical properties at high rates of strain. The blade fragment experiments reported herein were generated by single blade release. Single blade release is accomplished by properly notching a blade causing it to fail at the rotor's design operating speed.

Two types of blade containment experiments were conducted:

Single blade burst in which only one blade is mounted on a rotor disk and is modified to fail and produce a blade fragment.

Single blade bursts in which one blade in a fully bladed rotor is modified to fail.

The purpose of those experiments in which one blade in a fully bladed rotor was modified to fail was to define the interactions between the failed blade fragment and the remaining unfailed blades and subsequently to compare the results with those of the isolated blade experiments to determine what effect these interactions have on the containment process. The containment process was recorded by high-speed photography to provide the measurement of the ring and fragment displacements with respect to time. These data were used by MIT in their TEJ-2 computer program to obtain estimates of the force-time characteristics of the blade during the containment process. References 7 and 8 contain details of the TEJ-2 computer program.

Results of representative blade-fragment containment experiments are fully documented in reference 2. High-speed photography, used to characterize

the blade interactions during single blade failure in a fully bladed rotor, revealed that the remaining blades on the rotor impart added momentum to the failed blade thereby increasing its destructive potential. Although the containment rings used for the blade containment and disk containment tests were instrumented with strain gages, (as listed in table 1) the technique to acquire accurate data from the gages was not fully developed until test 201, therefore, their absolute values are of no significance.

DESCRIPTION AND DISCUSSION OF TEST 201

The techniques that were developed and the data analysed as a result of conducting the preliminary experiments were used to acquire better quality strain data and high speed photos in test 201. A trigger system was developed to activate the photo lighting system upon fragment release in order to provide a sequence of pictures prior to impact. The system consists of a continuous grounded circuit, which is maintained along a copper wire via a slip ring assembly to the photo lighting unit. A metalic contact pin, to which the copper wire is attached, maintains positive contact with the rotor bore until (lighting duration 2.7 millisec). A schematic of the trigger system is contained on page A-8.

Figures 2 & 3 are representative samples of the sequential photos that were obtained when recording the rotor fragment/ring interactions on high speed film. The permanent gross deformation experienced by the ring as a result of containment is shown in figure 4. The formation of three lobes on the ring are typical of a three fragment containment. The white dots shown painted on the ring's edge are trammel points used to measure, with the use of high-speed film, the transient displacements of the ring with respect to time.

An impact trigger, which was used in preliminary experiments to activate the lighting system, was used in test 201 to: (1) activate two oscilliscopes (single sweep), each of which recorded strain data from 2 gages; (2) indicate impact on FM tape in order to provide a zero time reference for all 10 strain measurements recorded on the FM tape. Strain gage locations and recording channel numbers are contained on pages A-9 and A-10.

The impact trigger consists of two parallel strips of electrically conductive foil tape attached to the inside surface of the containment ring. Upon impact, contact is made between the foil strips, thus completing the circuit. A circuit diagram and technical explanation of the system's operation are contained in appendix A. Pertinent pre- and post-test data acquired for test 201 are contained in appendix B.

The transient strain data recorded on FM tape is presented graphically in appendix C. The data was reproduced by playing the data stored on FM tape through a Biomation Model 1015 Waveform Recorder to an x-y plotter. This system provided resolution of the data that was not attainable from the oscilloscopes and therefore the scopes were only used as an assurance that the transient strains were being transmitted by the gages and recorded on the tape.

Four of the 10 strain gages survived the entire test. The permanent strains recorded from the four surviving gages (mass point locations 9, 13, 33 and 37) are presented in tabular form on page A-9. The maximum permanent strain recorded was 33,093 $\mu\epsilon$ in compression (see pages A-9 and A-10).

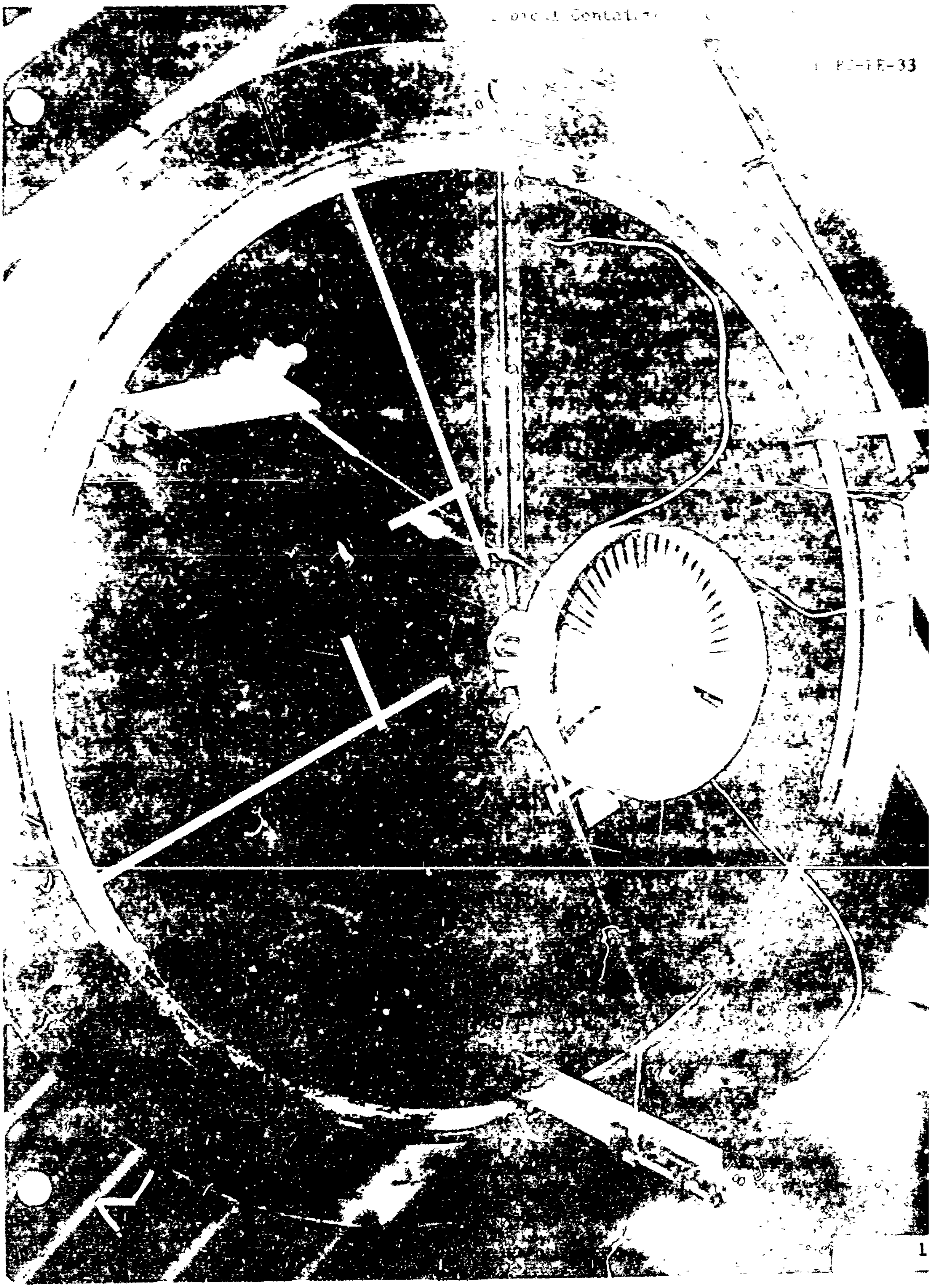

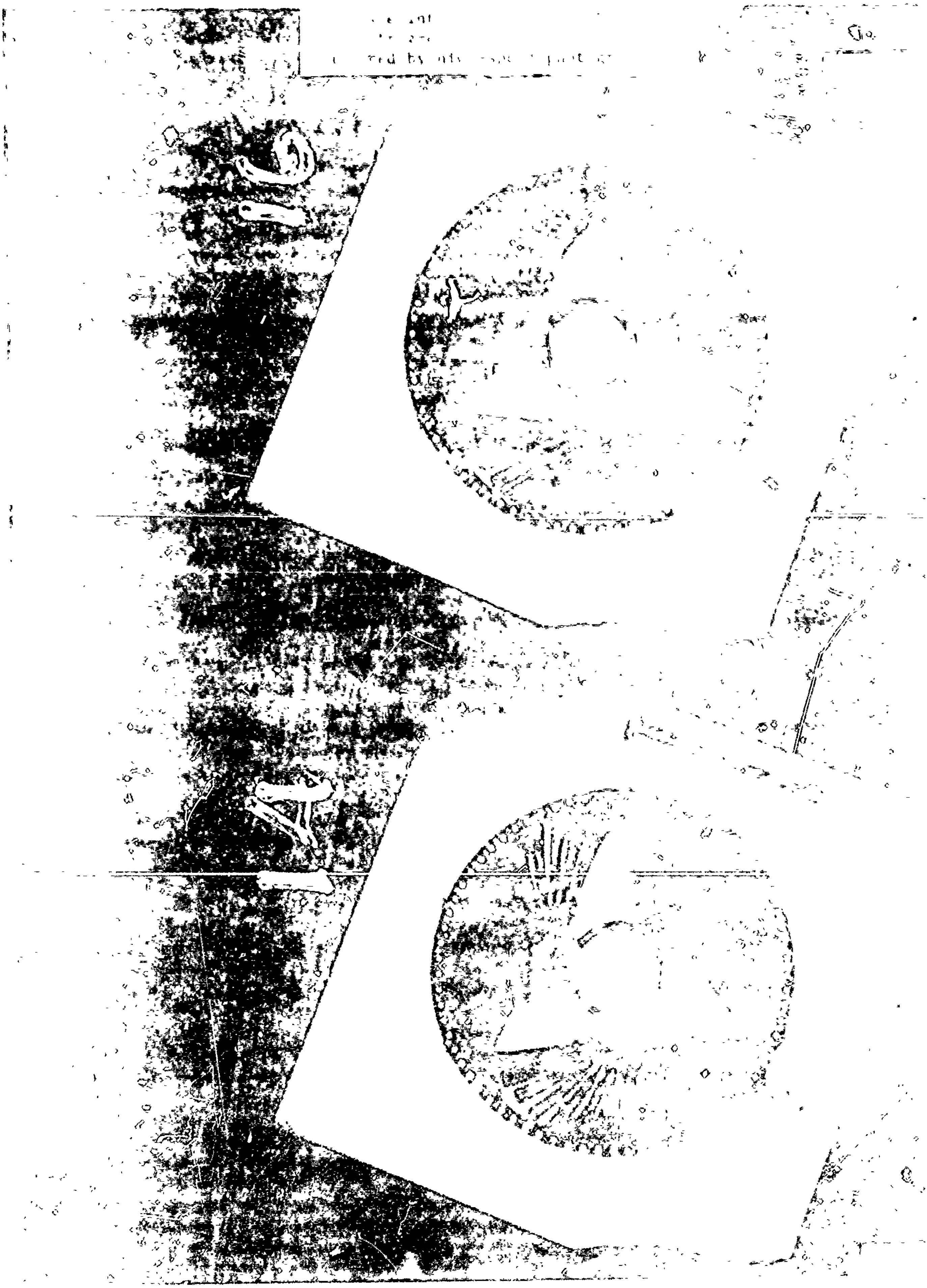

Hardware interaction during the three fragment rotor containment test captured by high-speed photography

NAPC-PE-

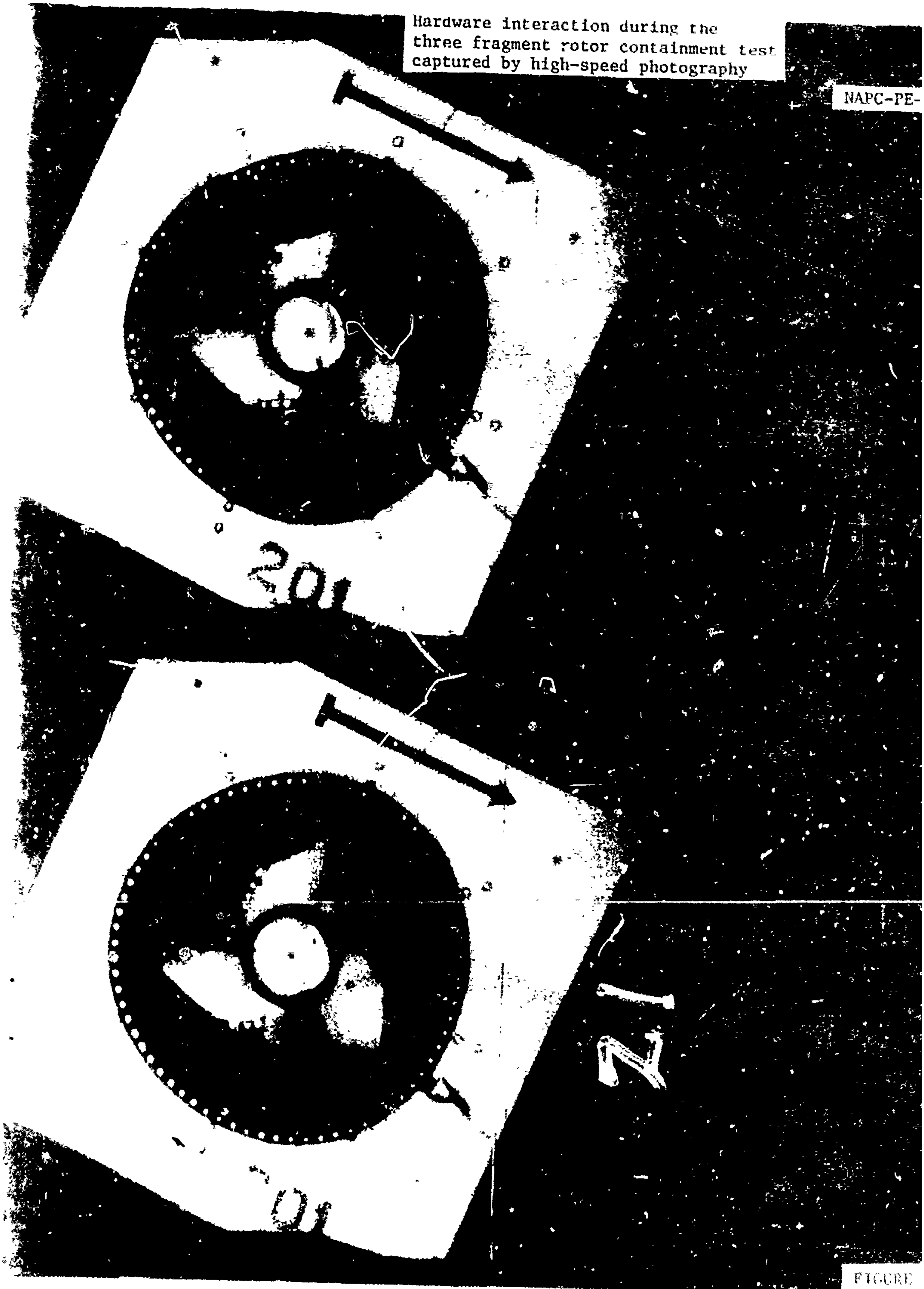

FIGURE

Permanent Deformation of
Containment Ring in Test 201

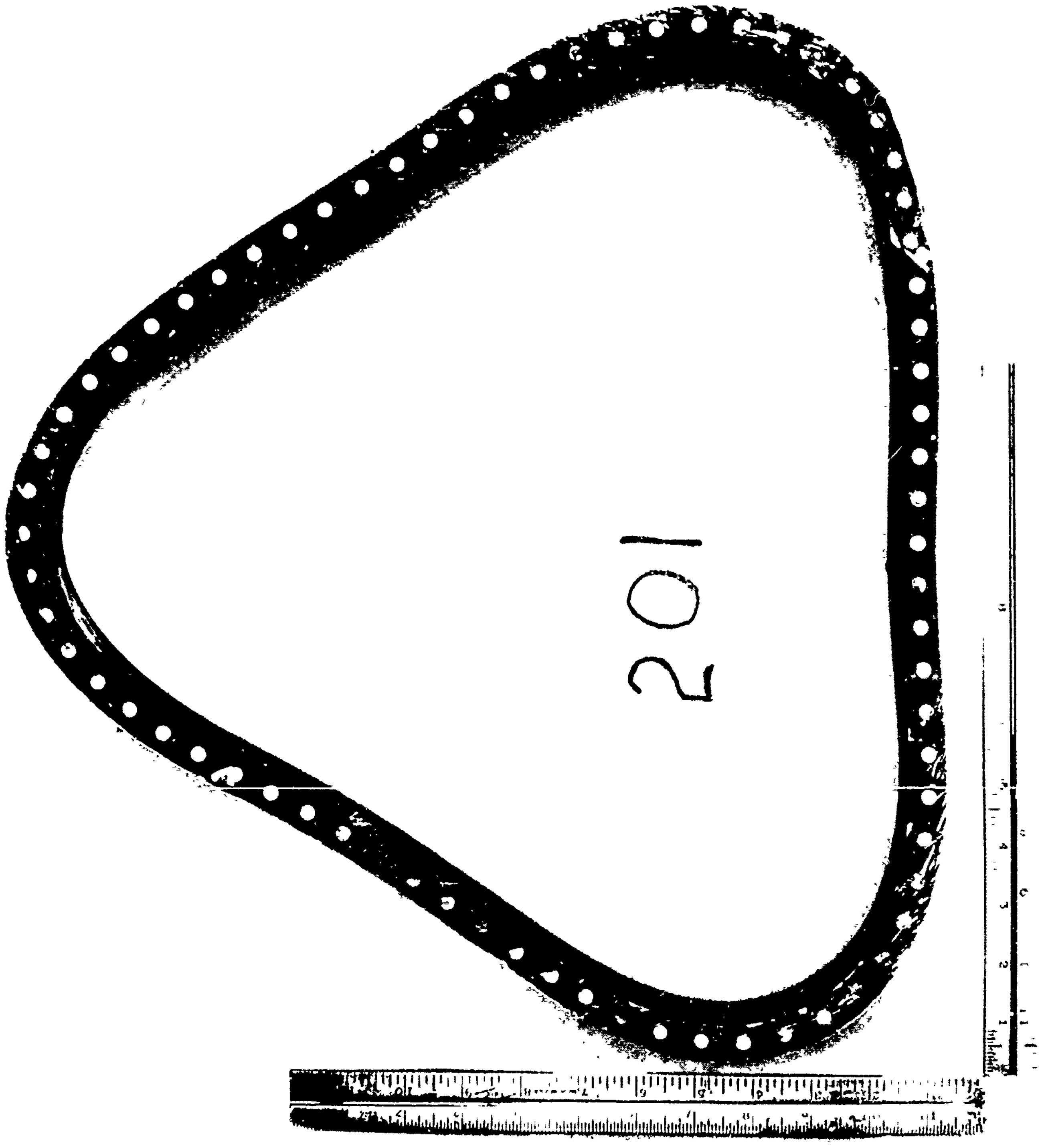

Figure 4

TABLE I

COMPILATION OF BLADE & ROTOR CONTAINMENT TEST WITH INSTRUMENTED CONTAINMENT RINGS

TEST NO.	DATE	TYPE OBJECTIVE TEST	ROTOR/DISK						CONTAINMENT/CONTROL						INSTRUMENTATION		RESULT
			TYPE	MATERIAL	DIAMETER INCHES	NO. OF FRAGMENTS	FAILURE SPEED RPM	TOTAL FRAGMENT ENERGY IN-LBS	CONFIG-URATION	MATERIAL	ID INCHES	THICKNESS INCHES	AXIAL LENGTH INCHES	WEIGHT LBS	HIGH SPEED PHOTOS	STRAIN MEAS.	
49	3-25-69	(1) BF	TURBINE ROTOR (3)	SEL	14.000	1	15500	6924	RING	6061-T6 AL	14.500	0.175	1.000	0.79	X	X	C
55	6-12-69	BF	TURBINE ROTOR (3)	SEL	14.000	1	15140	6624	RING	6061-T6 AL	14.500	0.175	1.000	0.82	X	X	C
57	7-11-69	BF	TURBINE ROTOR (3)	SEL	14.000	1	14580	6143	RING	6061-T6 AL	14.500	0.175	1.000	0.76	X	X	C
88	3-10-70	BF	TURBINE ROTOR (3)	SEL	14.000	1	15400	6854	RING	2024-T4 AL	17.313	0.173	1.506	1.46	X	X	C
91	3-18-70	BF	TURBINE ROTOR (3)	SEL	14.000	1	15650	7078	RING	2024-T4 AL	17.314	0.176	1.506	1.46	X	X	C
109	8-28-70	BF	TURBINE ROTOR (3)	SEL	14.000	1	15250	6420	RING	6061-T6 AL	14.999	0.156	1.508	1.10	X	X	C
111	9-21-70	BF	TURBINE ROTOR (3)	SEL	14.000	1	15820	7233	RING	6061-T6 AL	15.001	0.155	1.502	1.09	X	X	C
112	9-28-70	BF	TURBINE ROTOR (3)	SEL	14.000	1	15700	7124	RING	6061-T6 AL	15.005	0.148	1.502	1.10	X	X	C
114	10-19-70	BF	TURBINE ROTOR (3)	SEL	14.000	1	15700	7124	RING	6061-T6 AL	15.002	0.150	1.502	1.09	X	X	NC
146	10-14-71	BF	TURBINE ROTOR (3)	SEL	14.000	1	14800	6330	RING	6061-T6 AL	15.000	0.115	2.000	1.20	X	X	C
160	1-20-72	BF	TURBINE ROTOR (3)	SEL	14.000	1	15000	6503	RING	6061-T6 AL	15.000	0.155	2.000	1.30	X	X	C
161	2-1-72	BF	TURBINE ROTOR (3)	SEL	14.000	1	15234	6707	RING	6061-T6 AL	17.303	0.153	1.503	1.26	X	X	C
162	2-8-72	BF	TURBINE ROTOR (3)	SEL	14.000	1	14915	6429	RING	6061-T6 AL	17.302	0.154	1.502	1.23	X	X	C
165	4-12-72	BF	TURBINE ROTOR (3)	SEL	14.000	1	16286	7665	RING	6061-T6 AL	15.000	0.156	1.500	1.12	X	X	C
171	9-15-72	BF	TURBINE ROTOR (3)	SEL	14.000	1	16131	7520	RING	6061-T6 AL	15.084	0.1556	1.500	1.10	X	X	C
187	3-28-73	BF	TURBINE ROTOR (3)	SEL	14.000	1	15191	6669	RING	6061-T6 AL	15.000	0.1563	1.500	1.38	X	X	C

(1) Blade Failure
(2) Rotor Failure
(3) Turbine Rotor T-58 Engine, Axial Flow Power Turbine Rotor Tip to Hub Ratio = 2.147, Blade Material: SEL, Rotor Material : A=286
(4) 4130 Steel Billet #2 - Cast by Acipco

TABLE I (CONTINUED) COMPILATION OF BLADE & ROTOR CONTAINMENT TEST WITH INSTRUMENTED CONTAINMENT RINGS

TEST NO.	DATE	TYPE OBJECTIVE TEST	ROTOR/DISK						CONTAINMENT/CONTROL						INSTRUMENTATION		RESULTS
			TYPE	MATERIAL	DIAMETER INCHES	NO. OF FRAGMENTS	FAILURE SPEED RPM	TOTAL FRAGMENT ENERGY IN-LBS	CONFIG-URATION	MATERIAL	ID INCHES	THICKNESS INCHES	AXIAL LENGTH INCHES	WEIGHT LBS	HIGH SPEED PHOTOS	STRAIN MEAS.	
190	7-20-73	BF	TURBINE ROTOR (3)	SEL	14.000	1	15000	6503	RING	6061-T6 AL	15.000	0.1875	1.500	1.38	X	X	C
198	2-26-75	BF	TURBINE ROTOR (3)	SEL	14.000	1	16476	7845	RING	6061-T6 AL	15.000	0.250	1.500	1.76	X	X	NC
200	4-5-75	BF	TURBINE ROTOR (3)	SEL	14.000	1	15191	6669	RING	6061-T6 AL	15.000	0.250	1.500	1.77	X	X	NC
196	6-21-74	(2) RF	TURBINE ROTOR (3)	A286	14.000	3	20011	938564	RING	(4) 4130 STL	15.000	0.625	1.500	12.44	X	X	C
197	10-4-74	RF	TURBINE ROTOR (3)	A286	14.000	3	19882	926502	RING	(4) 4130 STL	15.000	0.625	1.500	13.00	-	X	C
199	3-22-75	RF	TURBINE ROTOR (3)	A286	14.000	3	20225	954745	RING	(4) 4130 STL	15.000	0.625	1.500	13.17	X	X	C
201	4-24-75	RF	TURBINE ROTOR (3)	A286	14.000	3	19857	924357	RING	(4) 4130 STL	15.000	0.625	1.500	12.83	X	X	C
202	5-2-75	RF	TURBINE ROTOR (3)	A286	14.000	3	20282	964166	RING	(4) 4130 STL	15.000	0.625	1.500	12.83	X	X	C

(1) Blade Failure
(2) Rotor Failure
(3) Turbine Rotor T-58 Engine, Axial Flow Power Turbine Rotor Tip to Hub Ratio = 2.147, Blade Material: SEL, Rotor Material: A=286
(4) 4130 Steel Billet #2 - Cast by Acipco

REFERENCES

1. REPORT - Mangano, G. J., Salvino, J. T. and DeLucia, R. A., "Rotor Burst Protection Program: Experimentation to Provide Guidelines For The Design of Turbine Rotor Burst Fragment Containment Rings". Naval Air Propulsion Test Center, NAPTC-PE-98 of March 1977

2. REPORT - Mangano, G. J., "Rotor Burst Protection Program - Phases VI and VII; Exploratory Experimentation to Provide Data For The Design of Rotor Burst Fragment Containment Rings", Naval Air Propulsion Test Center, NAPTC-AED-1968 of March 1972

3. REPORT - Martino, A. A. and Mangano, G. J., "Rotor Burst Protection Program - Final Phase V Report on Problem Assignment NASA DPR R-105", Naval Air Propulsion Test Center, NAPTC-AED-1901 of May 1969

4. REPORT - Martino, A. A. and Mangano, G. J., "Rotor Burst Protection Program - Final Phase IV Report on Problem Assignment NASA DPR R-105", Naval Air Propulsion Test Center, NAPTC-AED-1869 of April 1968

5. REPORT - Martino, A. A. and Mangano, G. J., "Turbine Disk Burst Protection Study", Final Phase II-III Report on Problem Assignment NASA DPR R-105", Naval Air Propulsion Test Center, NAPTC-AEL-1848 of February 1967

6. REPORT - Martino, A. A., "Turbine Disk Burst Protection Study - Final Phase I Report on Problem Assignment NASA DPR R-105", Naval Air Propulsion Test Center, NAEC-AEL-1793 of March 1965

7. REPORT - McCallum, R. B., Leech, J. W. and Witmer, E. A., "On the Interaction Forces and Responses of Structural Rings Subjected to Fragment Impart" - Interim Report, NASA CR-72801, ASRL TR 154-2, of September 1970

8. REPORT - Yeghiayan, Raffi P.; Leech, John w.; and Witmer, Emmett A.; "Experimental and Data Analysis Techniques for Deducing Collision-Induced Forces from Photographic Histories of Engine Rotor Fragment Impact/Interaction with a Containment Ring" MID ASRL TR 154-5 October 1973 (NASA CR-134548).

9. REPORT - Stagliano, Thomas R.; Spilker, Robert L.; and Witmer, Emmett A.; "User's Guide to Computer Program CIVM-JET 4B to calculate the Transient Structural Rings to Engine-Rotor-Fragment Impact" MIT ASRL TR 154-9 (NASA CR-134907).

APPENDIX A

EXPLANATION OF OPERATION

FOR

IMPACT TRIGGER AND STRAIN INSTRUMENTATION

AND

MEASURING SYSTEMS

EXPLANATION OF OPERATION OF IMPACT TRIGGER

The impact trigger used at NAPC for rotor failure tests is a transistor-transistor logic (TTL) circuit. All logic chips are of the 74 series designed for high-speed, general-purpose digital applications. A drawing of the circuit is provided on page A-6.

Prior to running, Z3 is cleared by depressing switch S2. To check the circuit switch, S1 is depressed. The Q output of Z3 should go from logical zero to logical one. On the output of Z4, a 70 microsecond pulse should be seen.

If the circuit checks good, depress switch S2 again, the Q output of Z3 should return to logical zero. The circuit is now ready to sense impact.

The trigger grid, located on the inside surface of the containment ring, consists of two parellel strips of electrically conductive foil tape. One strip is connected to the shield of the coaxial cable; the other to the center conductor. Upon impact, contact is made between the foil strips, thus the input of Z1 is grounded. The output of X1, an inverter, becomes logical one, causing the output of Z2 to become logical zero. A zero on the preset of Z3 sets its Q output to logical one. The Q output of Z3 is recorded on tape and also connected to the B input of Z4. A transition from logical zero to logical one on the B input of Z4 causes the output of Z4 to give a one-shot pulse. The external resistance and capacitance determine the pulse duration. 10,000 ohms resistance and .01 microfarad capacitance are selected values to give a 70 microsecond pulse width.

The pulse on the input of Z5 in turn is seen as a logical zero for a 70 microsecond duration of the output. The logical zero, essentially ground, parellels the 1000 ohm resistor with the one arm of the bridge circuit. The result is a 70 microsecond signal at Vout.

The output of Z5 is open-collector transistor. During the 70 microsecond pulse. the transistor is in a saturation. At other times it is in cut-off. When the transistor is in cut-off, the 10,000 resistor is essentially connected to an open circuit, thus it will have no effect on Vout.

Once the Q output of Z3 becomes logical one, it will remain at logical one until switch S2 is depressed, thus what happens to the foil strip after initial impact will not cause additional pulses at the output of Z4.

UNCERTAINTY OF INITIAL IMPACT

We have assumed that initial impact of the ring and contact between the foil strips are coincidental events. Transmission time for the signal to arrive at the input of the TTL circuit is less than 250 nanoseconds. The propagation time of the circuitry is as follows:

Z1 (low-to-high level output) 15 nanoseconds maximum

Z2 (high-to-low level output) 15 nanoseconds maximum

Z3 (delay time to logical one from preset to output) 25 nanoseconds maximum

Z4 (delay time to logical one from B input to Q output) 55 nanoseconds maximum

Z5 (high-to-low level output) 23 nanoseconds maximum

The cumulative effect of these delay times introduces no more than a 300-nanosecond error between the strain gage channels and the output of the impact circuit being recorded on tape. The signal superimposed on the strain gage channels will not be delayed more than 4 nanoseconds through the impact circuit.

To determine the propagation time through the signal conditioning amplifiers, a signal was applied to the input of the amplifier and the time delay between the input and output signal was noted. The time difference between the two signals was determined to be less than two microseconds.

If the time base error of the tape heads is corrected for, the time correlation between the impact channel and the strain channels should be within 2.5 microseconds.

UNCERTAINTY OF TRANSIENT STRAIN LEVELS

Immediately prior to failure, a two-point system calibration is recorded on tape. One calibration is ambient indicating no strain. The other point is a simulated strain obtained by placing a resistance in series with the strain gage. The value of resistance is determined by the desired calibration level and information provided by the strain gage manufacturer. The resistance is within .1 ohm of the calculated value introducing less than $\pm$ .5% error of reading.

When the data is played back and plotted, the calibrations are used to set up the proper span of the X-Y recorder.

A linearity error does exist when a strain gage is connected in a bridge configuration and the strain gage resistance changes significantly. This is shown mathematically below:

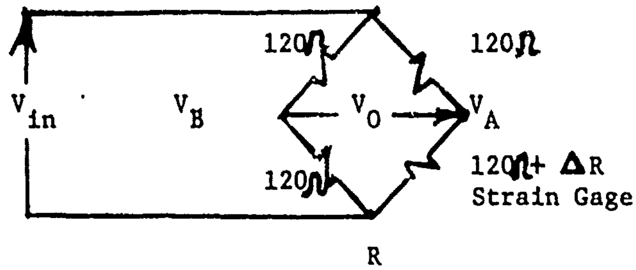

$$V_0 = V_A - V_B \qquad \frac{(120 + \Delta R)\, V_{in}}{120 + \Delta R + 120} = V_A$$

$$\frac{(120)}{(120 + 120)}\, V_{in} = V_B$$

$$1/2\ V_{in} = V_B$$

$$\frac{V_A - V_B}{V_{in}} = \frac{(120 + \Delta R)}{(240 + \Delta R)} - 1/2$$

$$= \frac{2(120 + \Delta R) - (240 + \Delta R)}{2(240 + \Delta R)}$$

$$V_0/V_{in} = \frac{\Delta R}{2\,(240 + \Delta R)}$$

One sees that as long as ΔR is neglibible compared to 240 ohms, then the relationship between ΔR and V_0/V_{in} is linear and the same follows for V_0/V_{in} and strain. The curve on page A-7 shows how the indicated strain deviates from the actual strain when a two-point calibration is performed with a ΔR of zero ohms and a ΔR of 19.6 ohms (80,000 microstrains). This error can be corrected by use of the theoretical curve on page A-7.

The strain gages are within $\pm$ 0.5% of reading. The signal conditioning amplifiers are within $\pm$ 0.1% of full scale.

The linearity of the tape recorder is within $\pm$ 0.3% of full scale deviation. The waveform recorder is accurate to within $\pm$ .1% of full scale. For example, full scale is 80,000 microstrains (in most cases 60,000 microstrains), the error is $\pm$ 400$\mu\epsilon$ $\pm$ (.005 + .005) X (strain level) assuming that the linearity error discussed above is corrected.

The worst case error would be at 30,000 microstrains in compression where 3500 + 400 + 30,000 X .01 = 4300 microstrains is possible if no corrections are made.

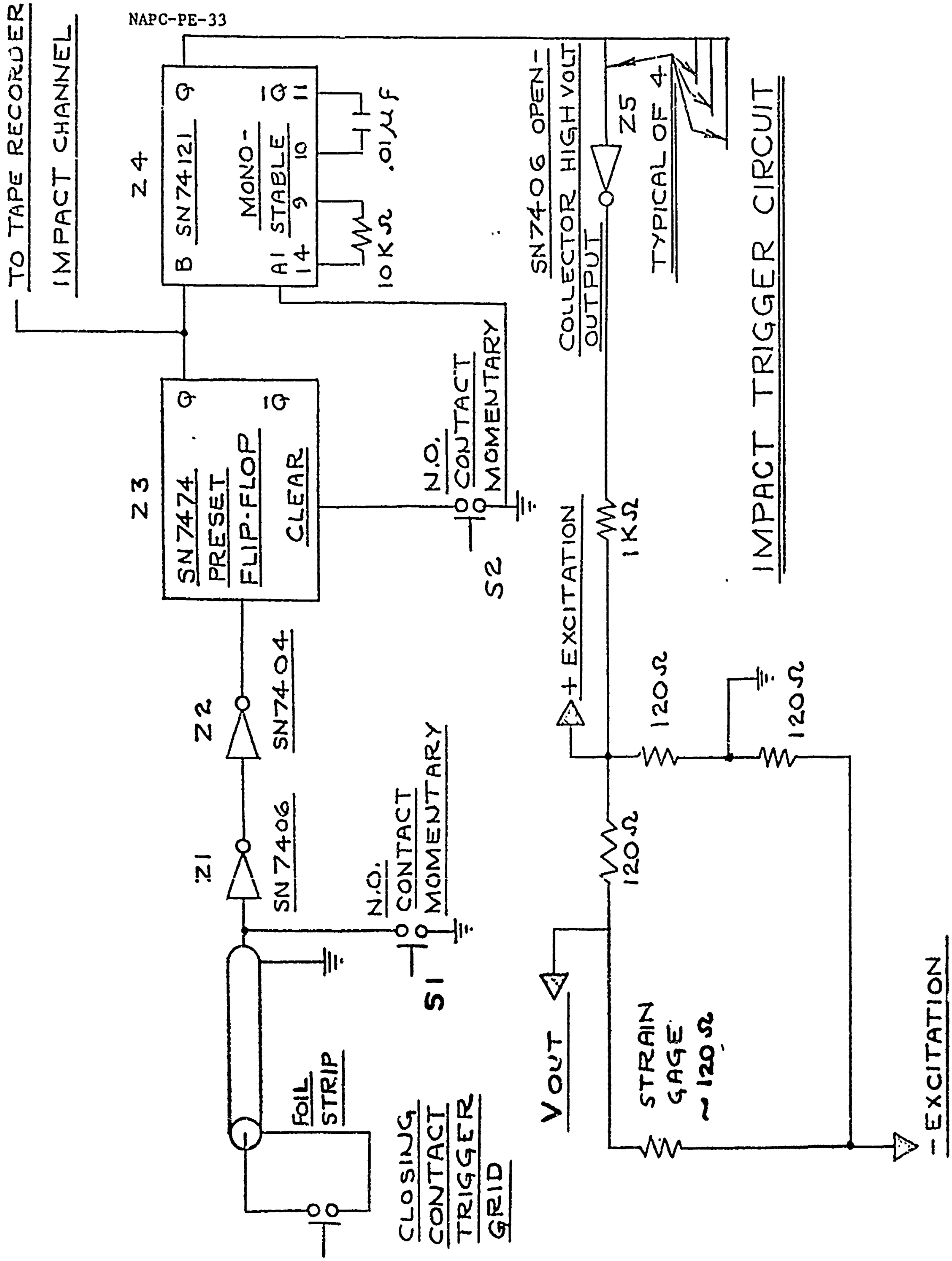

IMPACT TRIGGER CIRCUIT

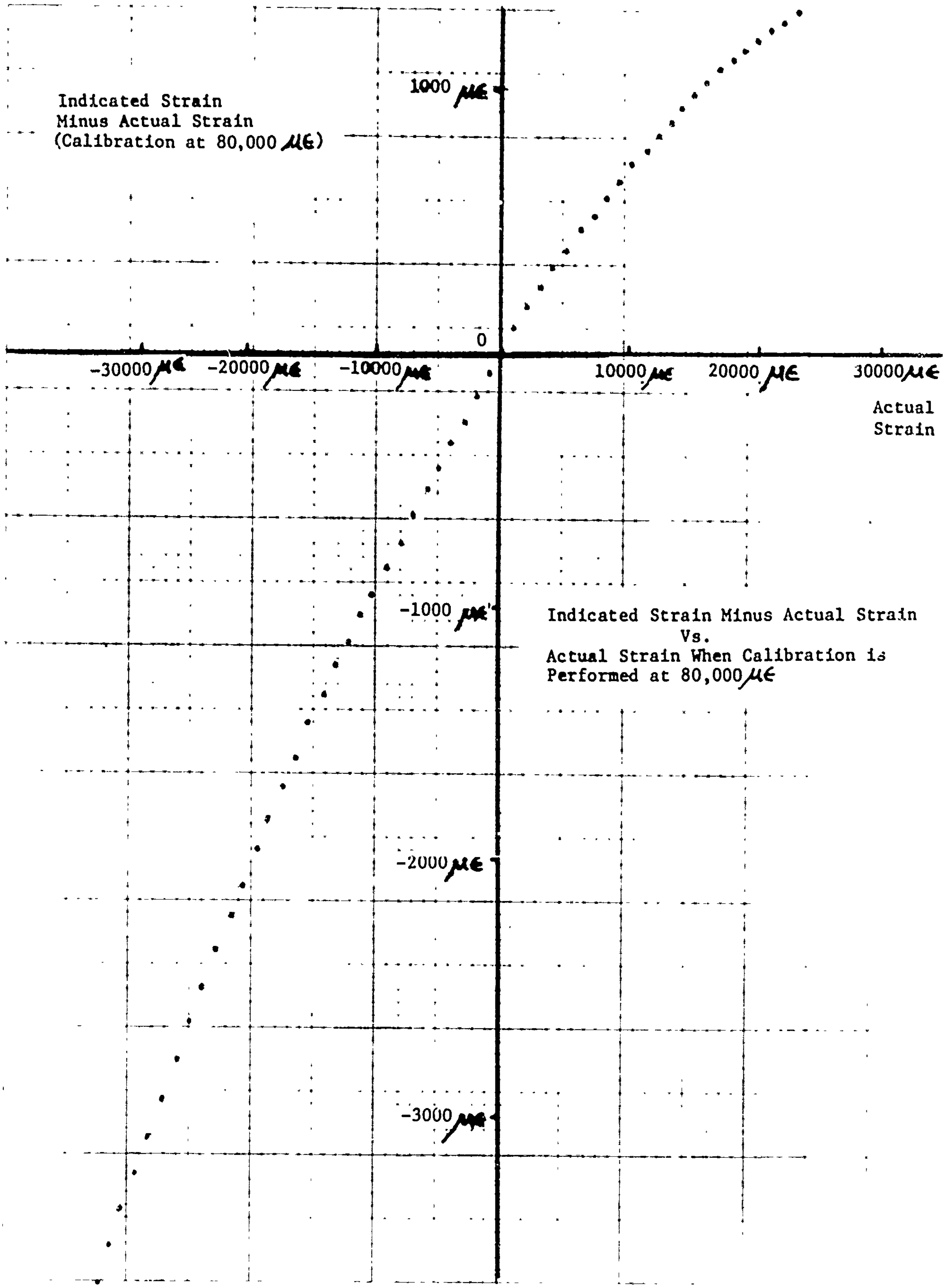
Indicated Strain
Minus Actual Strain
(Calibration at 80,000 με)
1000 με
0
-1000 με
-2000 με
-3000 με
-30000 με
-20000 με
-10000 με
10000 με
20000 με
30000 με
Actual
Strain
Indicated Strain Minus Actual Strain
Vs.
Actual Strain When Calibration is
Performed at 80,000 με

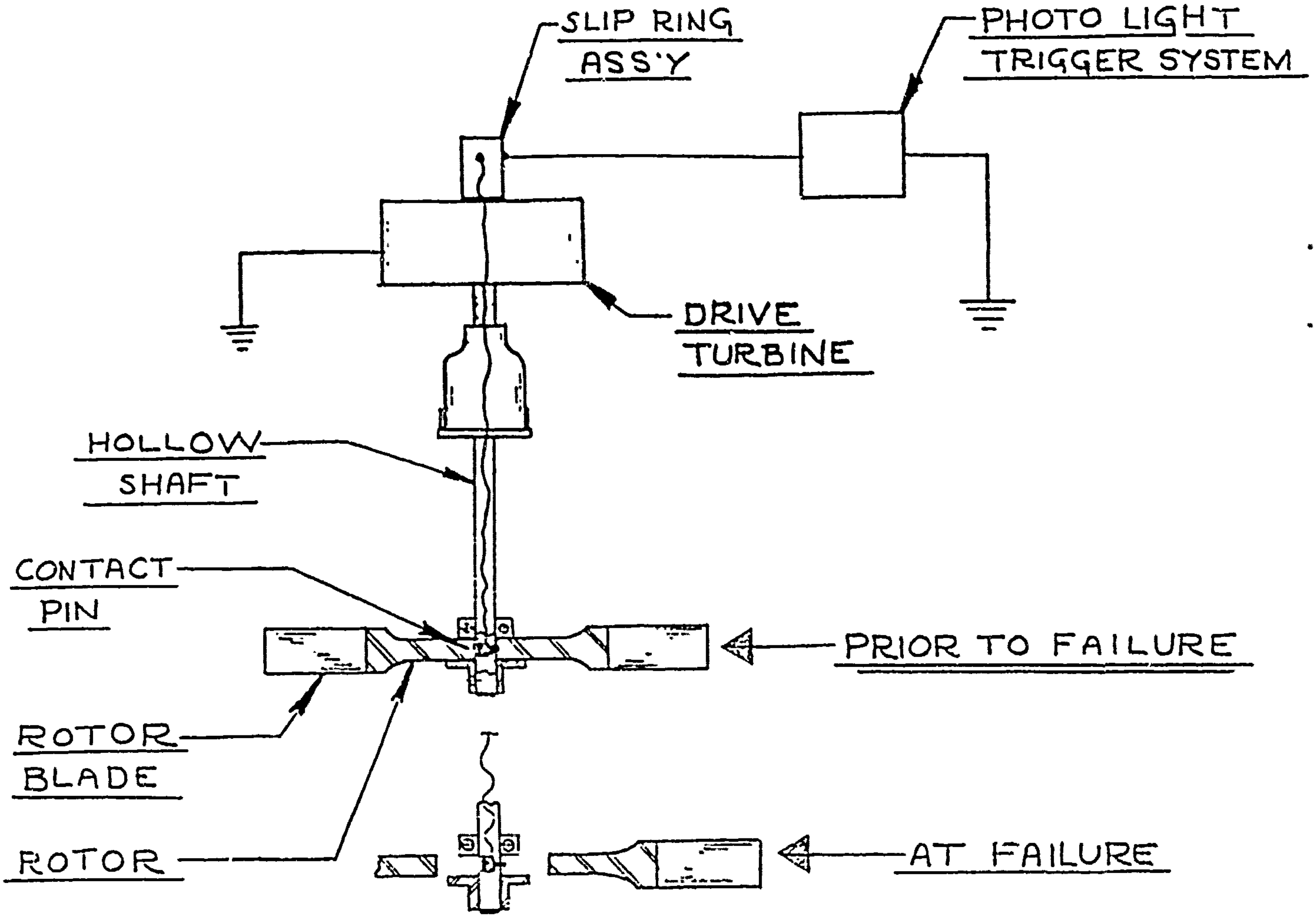

ROTOR FAILURE INDICATOR SCHEMATIC

BEFORE ROTOR FAILURE, CONTINUOUS GROUNDED CIRCUIT TO PHOTO LIGHTING UNIT MAINTAINED WITH CONTACT PIN AND ROTOR VIA SLIP RING ASSEMBLY.

WHEN ROTOR FAILS, CONTACT BETWEEN ROTOR AND CONTACT PIN IS BROKEN. THIS ACTION TRIGGERS PHOTO LIGHTING UNIT.

LABORATORY TEST SHEET

4ND-GEN-1128

LABORATORY NAPC-PE-33

TEST OF

TEST ENGINEER | OBSERVERS | DATE

TEST EQUIPMENT

RUN NO. 201 PERMANENT STRAIN DATA TEST 201

MASS POINT NO.	TAPE CHANNEL NO.	SCOPE CHANNEL NO.		PRE-TEST GAGE RESIST. OHMS	PRE-TEST CALIB. STRAIN $\mu\epsilon$	PRE-TEST CALIB. RESIST. OHMS		POST-TEST GAGE RESIST. OHMS	POST-TEST PERM. STRAIN $\mu\epsilon$	
1	9	1		118.5	60000	14.5		OPEN	--	
5	3	-		118.5	80000	19.3		OPEN	--	
9	4	-		118.1	60000	14.5		115.8	-9546	
13	10	2		118.5	60000	14.5		110.7	-32266	
17	5	-		118.7	80000	19.4		OPEN	--	
21	6	-		118.6	60000	14.5		OPEN	--	
25	11	3		118.5	60000	14.5		OPEN	--	
29	7	-		118.6	80000	19.4		OPEN	--	
33	1	-		118.6	60000	14.5		116.0	-10746	
37	12	4		118.5	60000	14.5		110.5	-33093	

GAGE DATA:

Rg (NOM) 120 OHMS

F (NOM) 2.04

TYPE* EP-08-250AF-120

FORMULA: $\epsilon = \frac{\Delta R}{Rg} \cdot \frac{1}{F}$

$R_{CAL} = RgF \times \mu\epsilon$

*Made by: Micro-Measurements, Division of Vishay Intertechnology Inc.

NAVY-NPS 4ND-PHILA., PA.

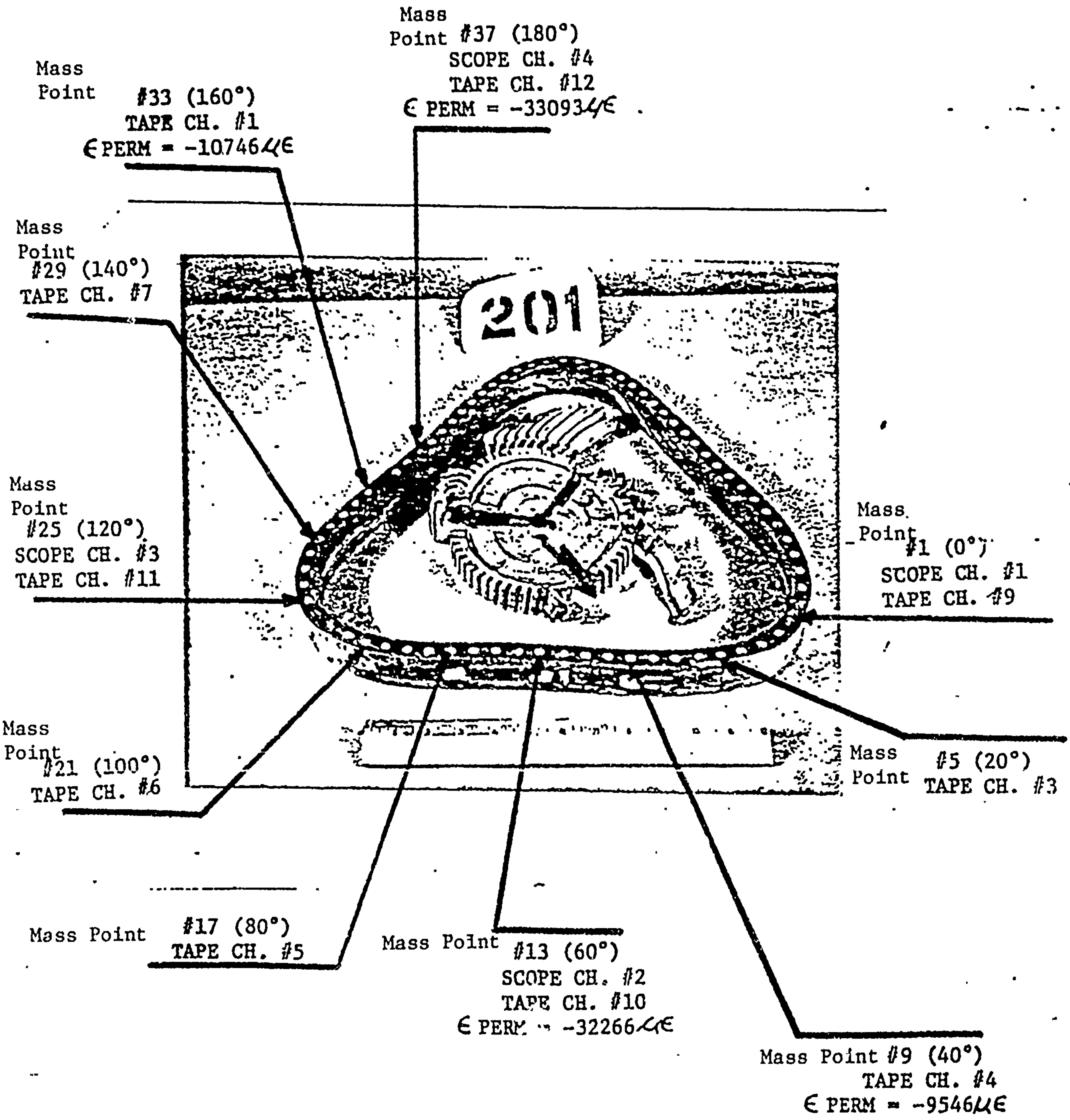
Mass Point #37 (180°)
SCOPE CH. #4
TAPE CH. #12
∈ PERM = -33093μ∈
Mass Point #33 (160°)
TAPE CH. #1
∈ PERM = -10746μ∈
Mass Point #29 (140°)
TAPE CH. #7
201
Mass Point #25 (120°)
SCOPE CH. #3
TAPE CH. #11
Mass Point #1 (0°)
SCOPE CH. #1
TAPE CH. #9
Mass Point #21 (100°)
TAPE CH. #6
Mass Point #5 (20°)
TAPE CH. #3
Mass Point #17 (80°)
TAPE CH. #5
Mass Point #13 (60°)
SCOPE CH. #2
TAPE CH. #10
∈ PERM = -32266μ∈
Mass Point #9 (40°)
TAPE CH. #4
∈ PERM = -9546μ∈

APPENDIX B

ROTOR CONTAINMENT

TEST 201

ROTOR FRAGMENT AND CONTAINMENT RING

PRE AND POST TEST DATA

NAPC-PE-33

LABORATORY TEST SHEET

4ND-GEN-1128

LABORATORY: RFPP

TEST OF: RING MEASUREMENTS TEST # 201

TEST ENGINEER | OBSERVERS | DATE

TEST EQUIPMENT

MASS POINT NO.	RING TH'K IN.	MASS POINT NO.	RING TH'K IN.	MASS POINT NO.	RING TH'K IN.	MASS POINT NO.	RING TH'K IN.		INSIDE DIAMETER MASS POINT	TO	MASS POINT	DIA IN.
* #1 1(0°)	.612	24	.622	47	.628	70	.613		1	TO	37	15.050
2	.617	* #3 25	.622	48	.631	71	.612		5	TO	41	15.031
3	.618	26	.620	49	.633	72	.613		9	TO	54	15.020
4	.621	27	.621	50	.638				11	TO	47	15.010
5	.625	28	.622	51	.639				13	TO	49	15.000
6	.630	29	.621	52	.642				17	TO	53	14.986
7	.632	30	.619	53	.641				21	TO	57	14.987
8	.632	31	.618	54	.641				25	TO	61	15.011
9	.633	32	.614	55(270°)	.641				29	TO	65	15.020
10	.631	33	.614	56	.639				31	TO	67	15.035
11	.360	34	.615	57	.639				33	TO	69	15.045
12	.628	35	.612	58	.635							
* #2 13	.628	36	.613	59	.632		RING	WT. =	12.83	LBS		
14	.627	* #4 37(180°)	.613	60	.631							
15	.628	38	.611	61	.628		ROTOR	WT. =	10.88			
16	.627	39	.612	62	.627							
17	.626	40	.610	63	.624		* DENOTES GAGES INSTALLED					
18	.632	41	.612	64	.623		TO READ THROUGH SCOPES -					
19(90°)	.630	42	.612	65	.621		REMAINDER ARE TO BE READ					
20	.629	43	.612	66	.617		THROUGH TAPE					
21	.628	44	.615	67	.619							
22	.628	45	.617	68	.614							
23	.626	46	.621	69	.614							

Test No. 201

Date 24 APRIL 1975

Results

Description TRI-HUB FAILURE VS. STEEL RING

Objective

Rotor Used T-58

Containment Used CYLINDRICAL RING

FRAGMENT GENERATOR		
Type Fragments	---	PIE SECTOR
No. Fragments	---	3
Fragment Weights	lbs	3.627
Fragment Center of Mass	inches	2.7969
Failure Speed	rpm	19859
CONTAINMENT DEVICE		
Type	---	RING
Material	---	4130 STEEL (CAST)
Radial Thickness	inches	0.6250
Axial Length	inches	1.500
I.D.	inches	15.000
Weight	lbs	12.83
Support Mode	---	TRI-WIRE

RUN NO.	201	
TARGET DATE	11 MARCH 1975	RUN DATE 24 APRIL 1975
CONTROL DEVICE		
MAT'L.	4130 A CAST STEEL (ACIPCO 2 BILLET)	
GEOM.	CYLINDRICAL	
DIMENSIONS	I.D. 15.0 INCHES O.D. 16.250 INCHES t 0.625 INCHES AL 1.5 INCHES	
SUSPENSION	TRI-WIRE	
INSTR.	HIGH SPEED PHOTOS	
MARKINGS	72 1/4 INCHED CODIT DOTS ON A BLACK BKGD.	
WEIGHT	12.83 LBS	
HARDNESS	332 BHN	
MISC.		
FRAGMENT GENERATOR		
ORIGINAL USE	T-58	
TYPE	AXIAL FLOW	
MAT'L.	A-286	
DIMENSIONS	14 INCHES O.D.	
RADIUS RATIO		
NO. FRAGMENTS	3	
FRAGMENT SHAPE	PIE SECTOR	
FRAGMENT WEIGHT	10.88 RPM	
HARDNESS		
DESIGN FAILURE SPEED	20000 RPM	
CENTROIDAL DISTANCE	2.797 INCHES	
MARKINGS		
MISC.	SEE SKETCH	

HIGH SPEED PHOTO SYSTEM:	TEST NO. 201
CAMERA	MODEL 350 S/N 119
LENS SETTING	
STOP SIZE	3/8 INCHES
CAMERA TO LID DIST.	
FRAMING RATE	35000 PPS
SPATIAL	
FCD SURFACE TO LID DISTANCE	
FRAG. GEN. SURFACE TO LID DISTANCE	
LIGHTING	
DURATION	2.7 MILLISEC
LIGHT TO LID DIST.	
NO. LIGHTS	2
REFLECTOR	CORDIN (NEW)
TRIGGER MODE	OPEN CONTACT
TRIGGER GRID	SHAFT BUTTON SWITCH
FILM:	
TYPE	KODAK TRI-X
DEVELOPMENT	DK-50 6 MIN. @ 70°F
IMPACT STRAIN MEASURING SYSTEM	BELL & HOWELL/CEC FM TAPE RECORDER
BRIDGE POTENTIAL	
TRIGGER MODE	CLOSING CONTACT

CHAN. NO.	SENSITIVITY	SWEEP RATE	INTENSITY
1			
2			
3			
4			

TRANSDUCER USED	

RESULTS AND ANALYSES

	VARIABLE/PARAMETER	VALUE	UNITS
N	Failure Speed	19859	PPM
Vc	Centroid Speed	5816.70	IPS
Vt	Tip Speed	14359.39	IPS
KE	Failure Energy	924357.914	IN-LB
M	Failure Momentum	444.484	IN-LB-SEC
Wr	Containment Ring Weight	12.83	LBS
KE/Wr	= SCFE	72046.532	IN-LB/LB

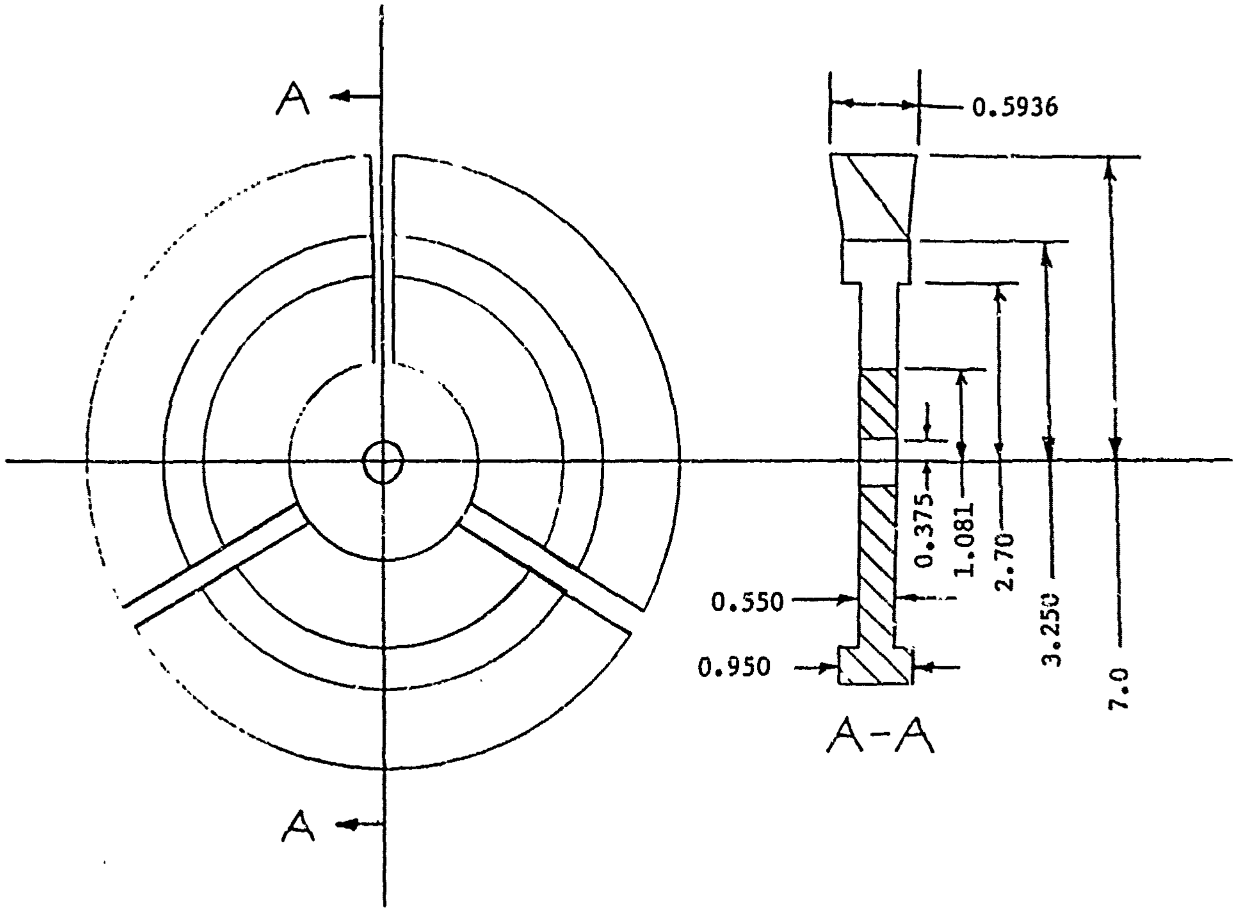

TYPE ROTOR: T-58 Power Turbine

DESCRIPTION: 3 fragment modification

ROTOR WEIGHT: 10.68 lbs

FRAGMENT CENTROIDAL DISTANCE: 2.797 in

FRAGMENT INERTIA: 47.9 lb-in^2

		DISK	BLADES
MATERIAL:		A-286	SEL-15
PROPERTIES:			
	SU	157K Psi	136K Psi
	SY	110K Psi	118K Psi
	EU	12%	12%
	HD	313 BHN	313 BHN

FIGURE 1

FRAGMENT DATA - TEST 201

A. Fragment Mass:

	Pre-Test	Post-Test
Fragment No. 1	3.627 lbs.	2.94 lbs.
Fragment No. 2	3.627 lbs.	2.07 lbs.
Fragment No. 3	3.627 lbs.	1.83 lbs.

B. Polar Moment of Inertia:

Fragment 1	54.9 $lb\text{-}in^2$	-
Fragment 2	54.9 $lb\text{-}in^2$	-
Fragment 3	54.9 $lb\text{-}in^2$	-
Total Rotor Inertia	164.7 $lb\text{-}in^2$	-

C. The CG Location of Each Fragment:

Fragment 1	2.80 in.	2.63 in.
Fragment 2	2.80 in.	2.03 in.
Fragment 3	2.80 in.	1.86 in.

1. $\pm$0.02 scatter for pre-test and post-test conditions.
2. All dimensions are from the shaft's axis.

D. CG Shift:

	x Axis		y Axis		O (deg)	
	Pre-Test	Post-Test	Pre-Test	Post-Test	Pre-Test	Post-Test
Fragment 1	0	0.41	0	0.20	0	8.90
Fragment 2	0	0.06	0	0.77	0	1.78
Fragment 3	0	0.06	0	0.94	0	1.94

E. Refer to Figure 1 for dimensions of fragments.

F. The Kinetic energy imparted by the rotor in Test 201 was 924,357 in-lbs. Therefore, the kinetic energy imparted by each fragment was 1/3 of the total or 308,119 in-lbs.

G. The ring used in Test 201 was manufactured from the Acipco 2 billet. Stress vs strain measurement data from specimen tests are presented in tabular form on page B-9 and B-10.

H. The background board in Test 201 was 2" behind the front face (with dots) of the ring.

RESULTS OF MECHANICAL TEST

Material: Thickness of Cast Cylinder

Grade: 4130

Original Form: Small Acipo II Casting

		Specimen No. 1	Specimen No. 2
Diameter of Specimen		.505	.505
Cross Sectional Area	(in^2)	0.20	0.20
*Yield Load	(lbs)	18,000	19,000
Tensile Load	(lbs)	21,750	23,000 (Max. @ Failure)
Elong. in 2"	(in)	0.32	0.32
Yield Strength	(Psi)	90,000	95,000
Tensile Strength	(Psi)	108,750	115,000
% Elong. 2"		16.0	16.0
% Red. in Area		44.9	40.4

*0.2% Offset.

TABULATED DATA

Specimen No. 1

Stress (σ (Psi))	Strain (E $\mu\epsilon$))
83,750	800
87,500	1600
90,000	2800
91,875	4000
108,750	160,000

Specimen No. 2

Stress (σ (Psi))	Strain (E $\mu\epsilon$))
87,500	1500
91,250	2000
95,000	3500
97,500	6000
98,750	8000
115,000	160,000

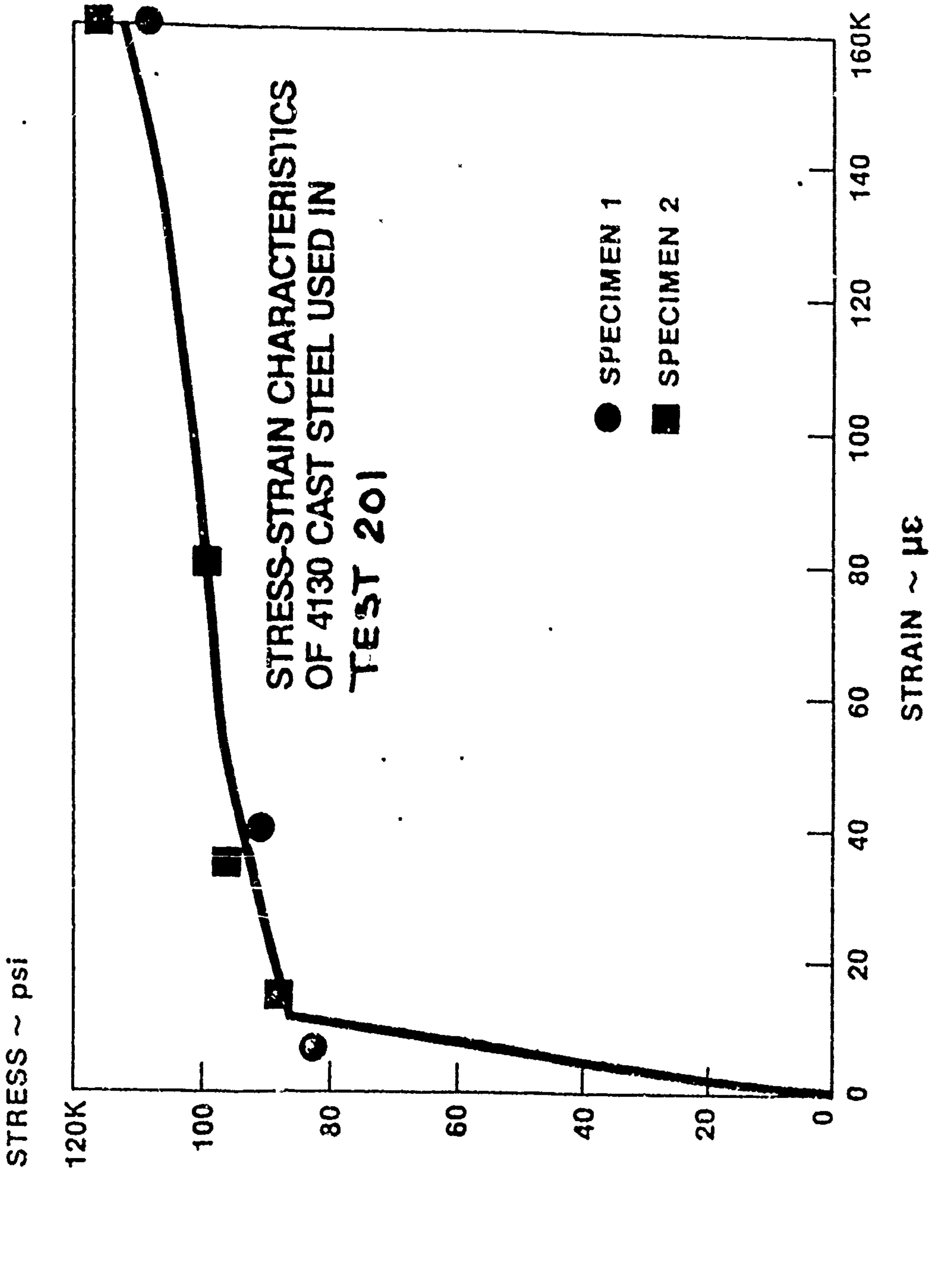
STRESS-STRAIN CHARACTERISTICS
OF 4130 CAST STEEL USED IN
TEST 201
● SPECIMEN 1
■ SPECIMEN 2
STRESS ~ psi
120K
100
80
60
40
20
0
STRAIN ~ με
0
20
40
60
80
100
120
140
160K

APPENDIX C

TEST 201

TRANSIENT STRAIN

VS

TIME TRACES REPRODUCED FROM FM TAPE

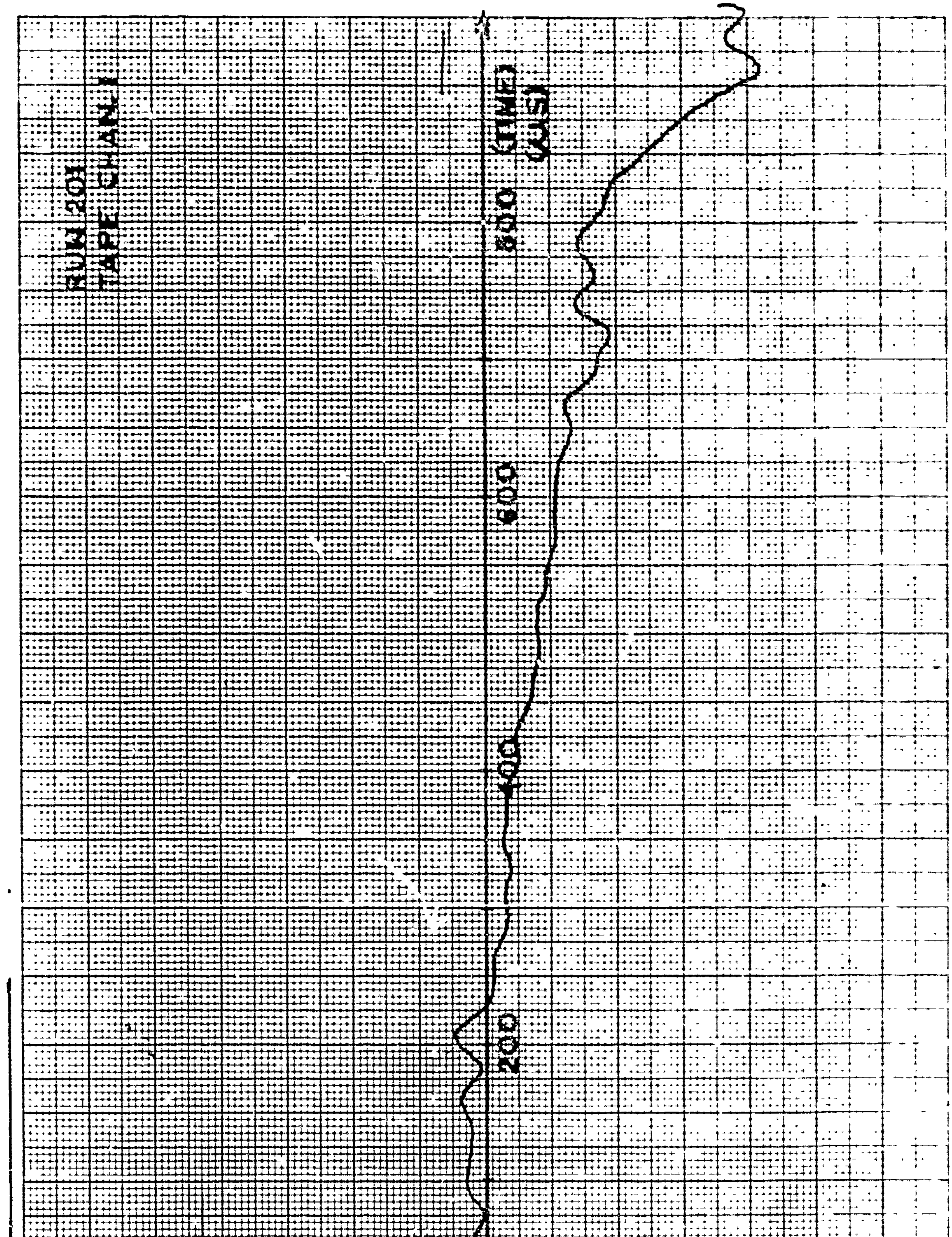
RUN 201
TAPE CHAN. I
800 (TIME) (μS)
600
400
200
TENSION (με X 1000)
20
10
0
10
20

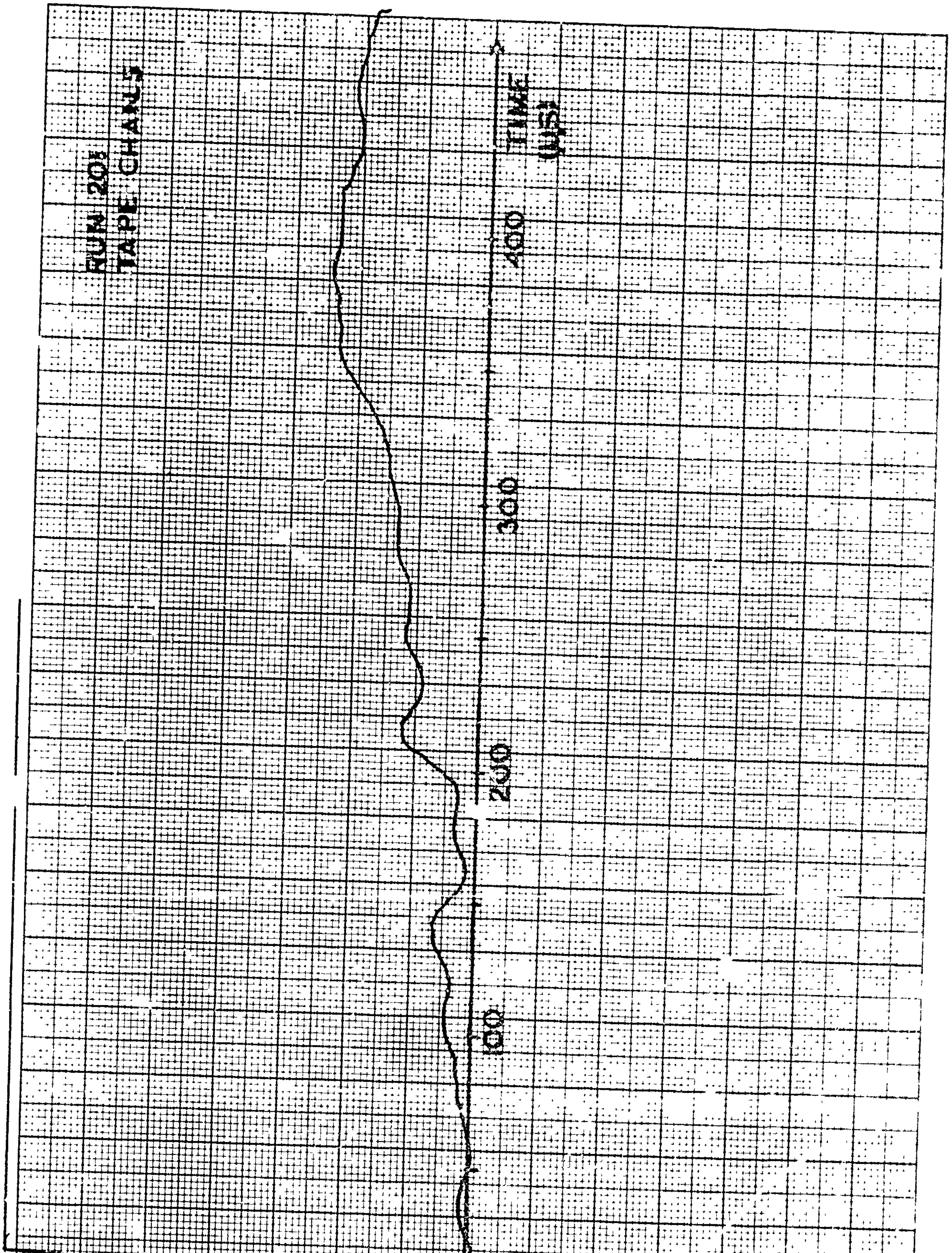
RUN 205
TAPE CHAN 5
TIME
(μS)
400
300
200
100
TENSION
(μE x 100)
10
5
0
5
10

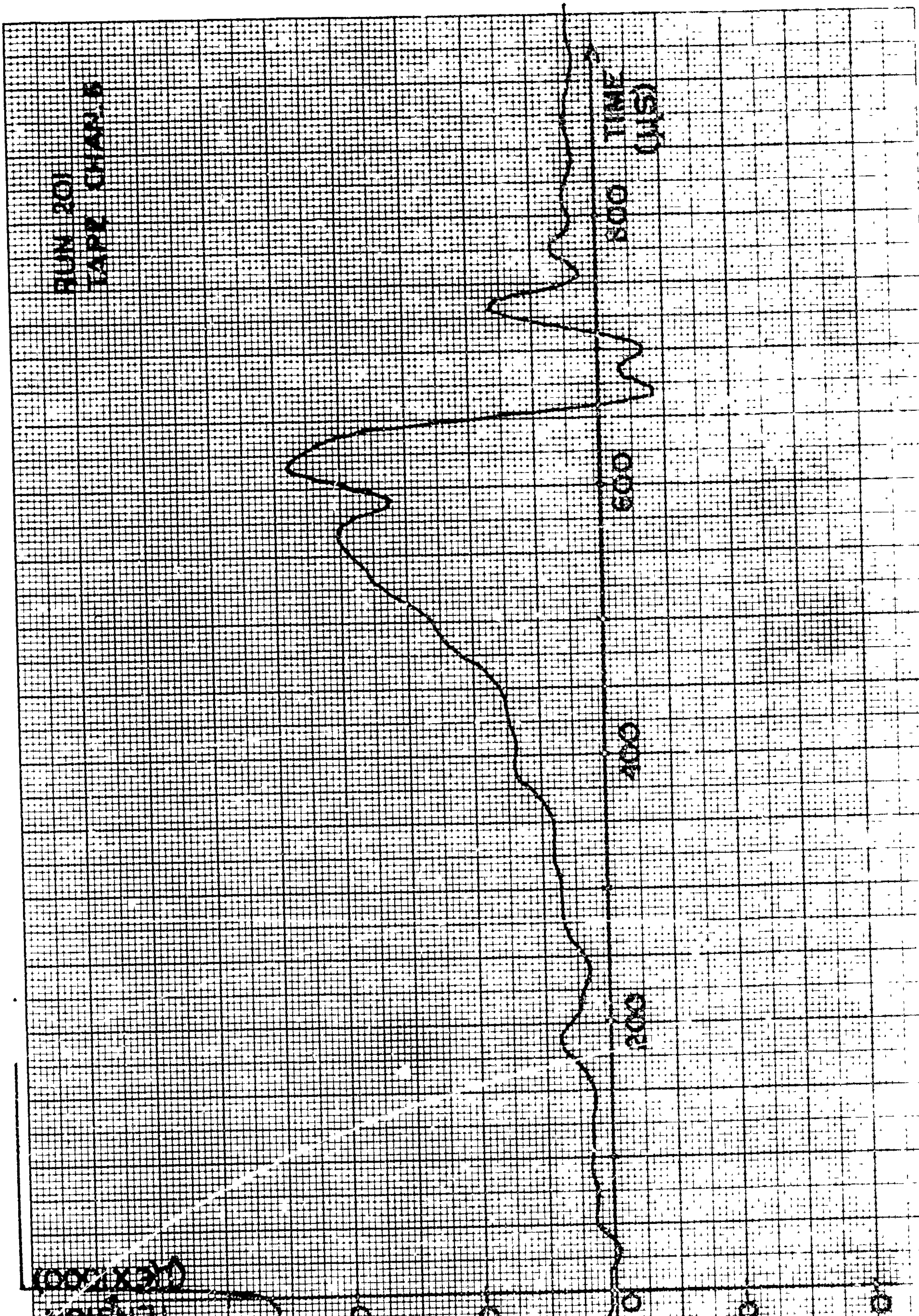
RUN 201
TAPE CHAN. 5
TIME (µS)
200
400
600
800
TENSION
20
10
0
10
20

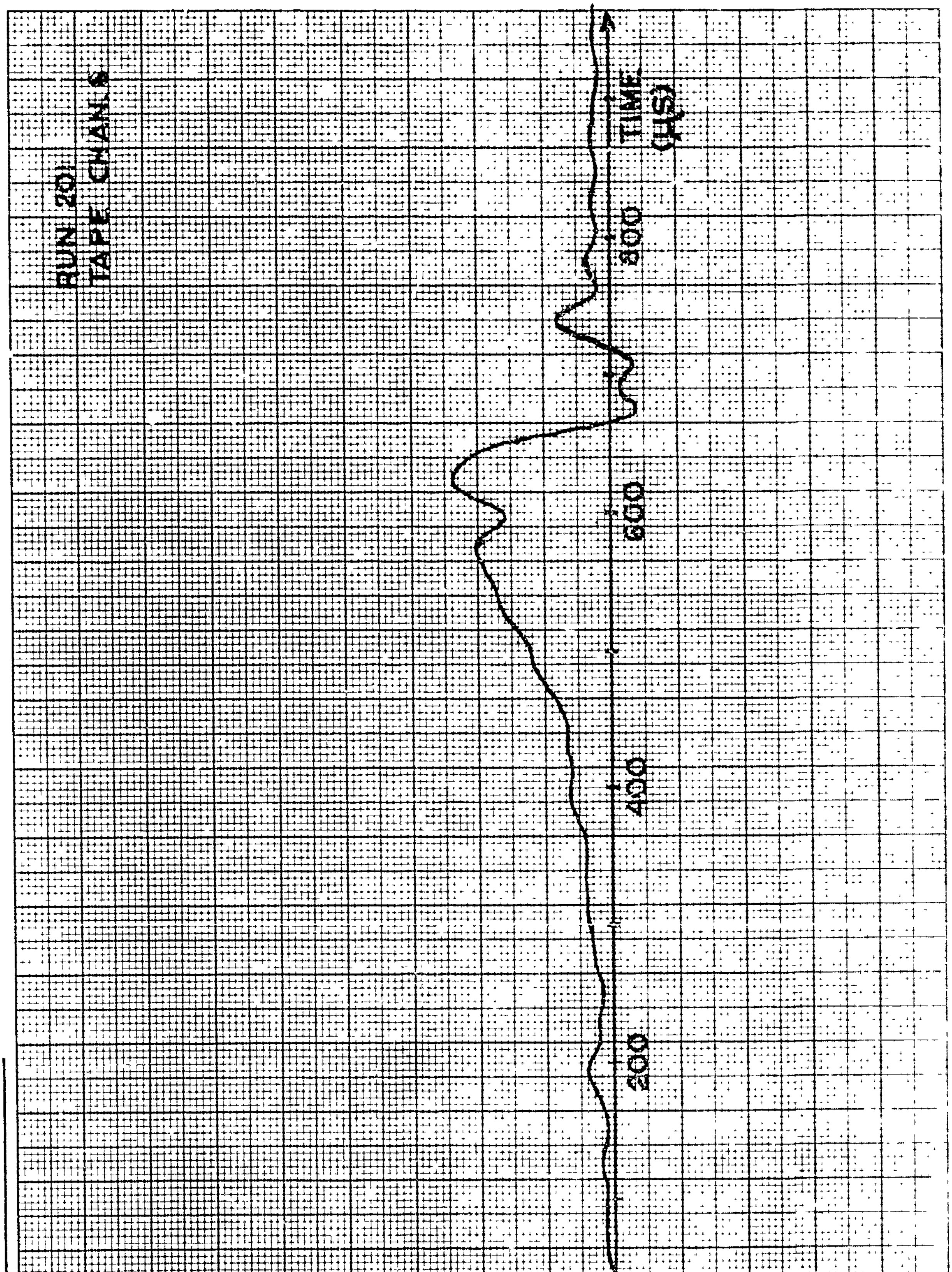
RUN 201
TAPE CHAN. 8
TIME
(μS)
800
600
400
200
0
TENSION
(με X 100)
60
40
20
20
40

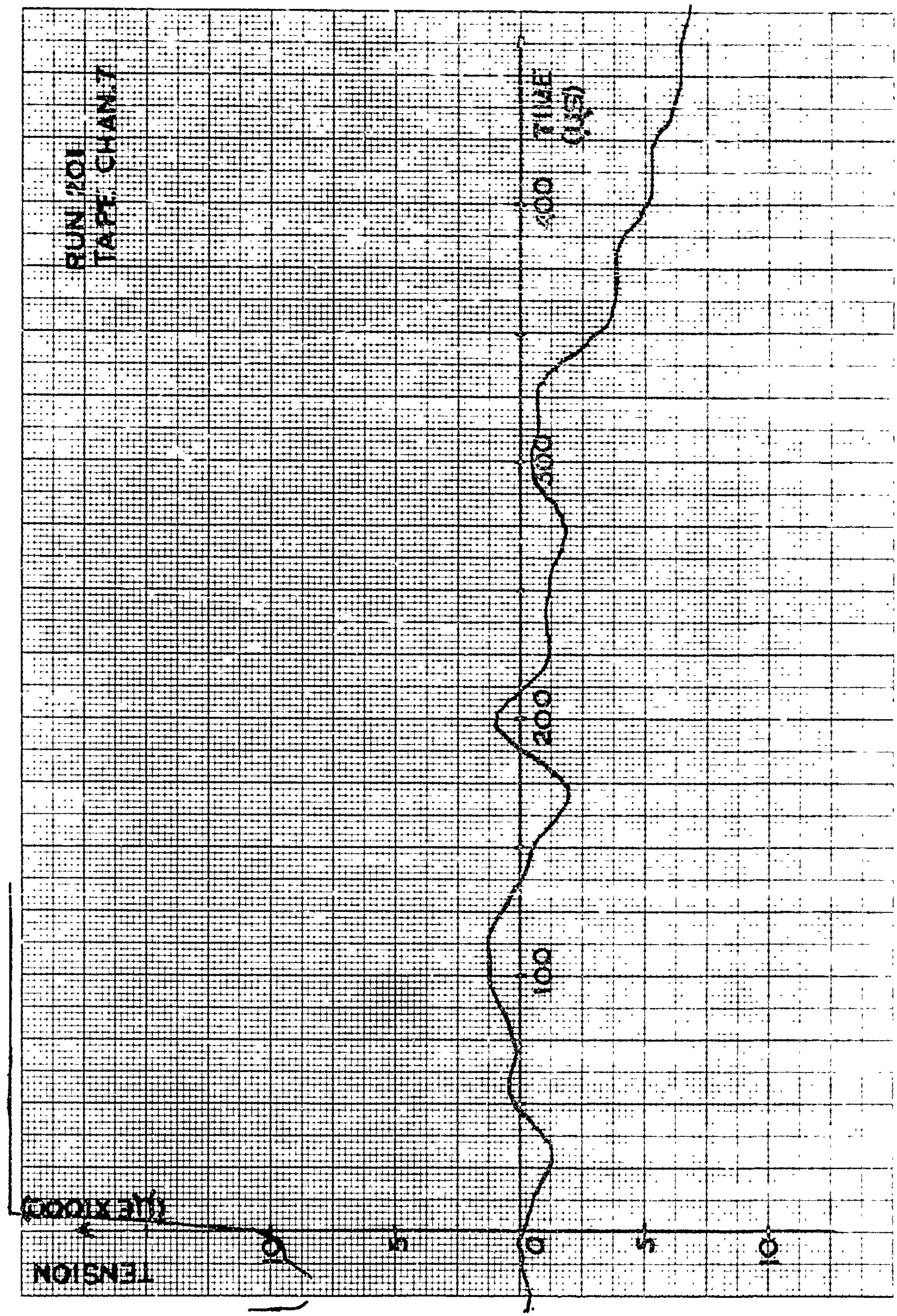
RUN 201
TAPE CHAN.7
TIME
(μS)
400
300
200
100
TENSION
(με X1000)
10
5
0
5
10

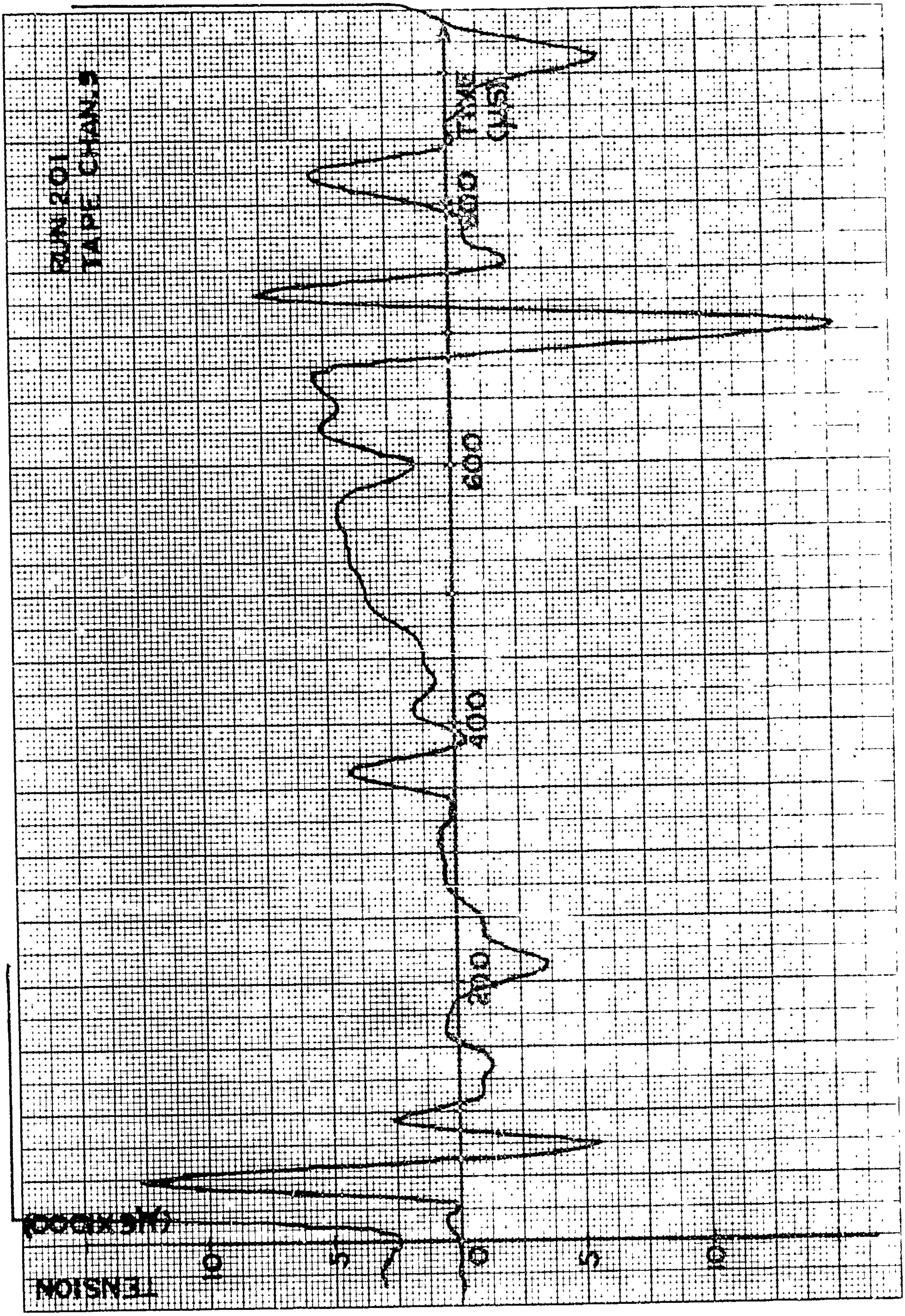
RUN 201
TAPE CHAN.5
TIME (µS)
800
600
400
200
TENSION
(µε x 1000)
10
5
0
5
10

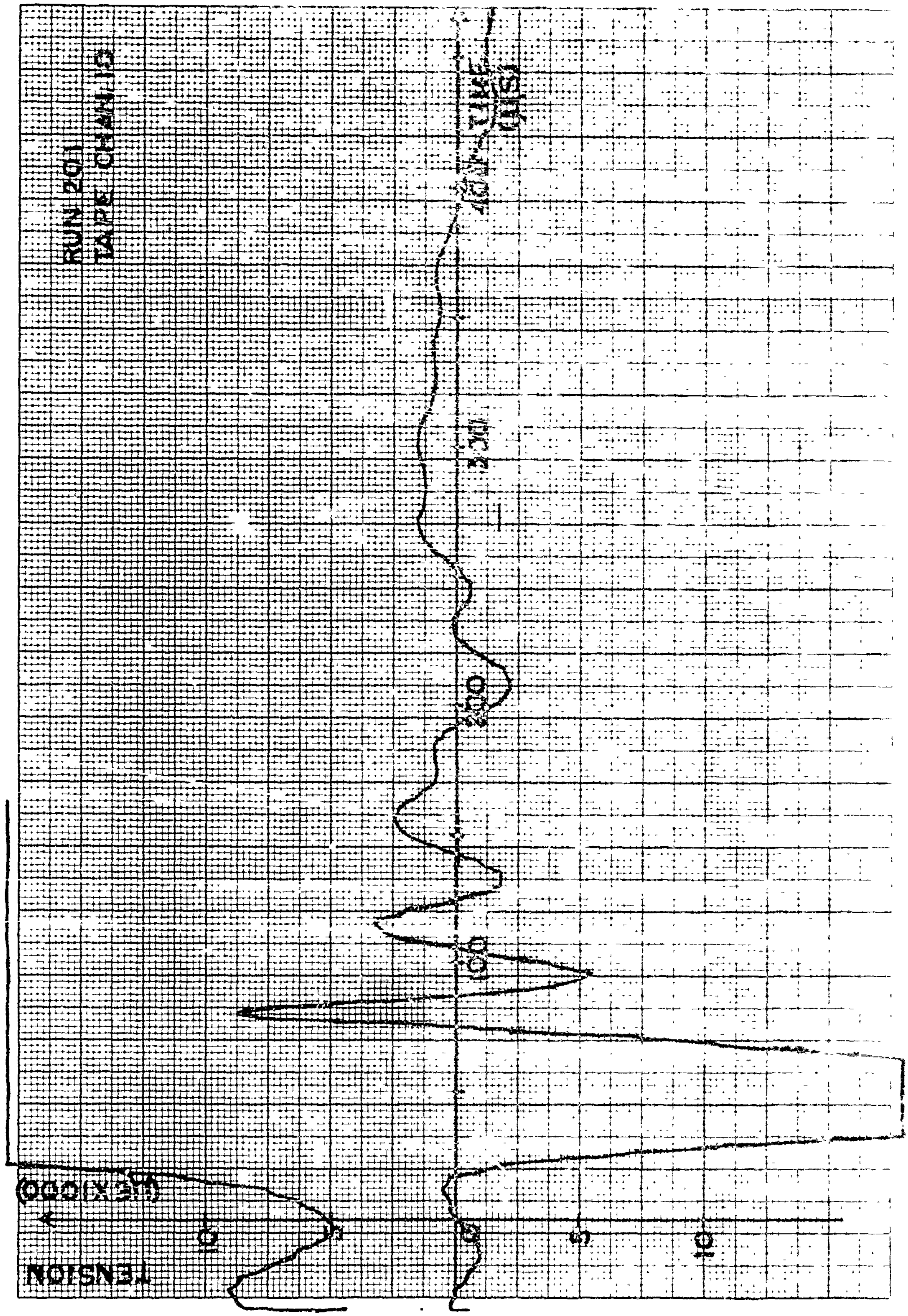
RUN 201
TIME (MS)
TENSION (LB X1000)

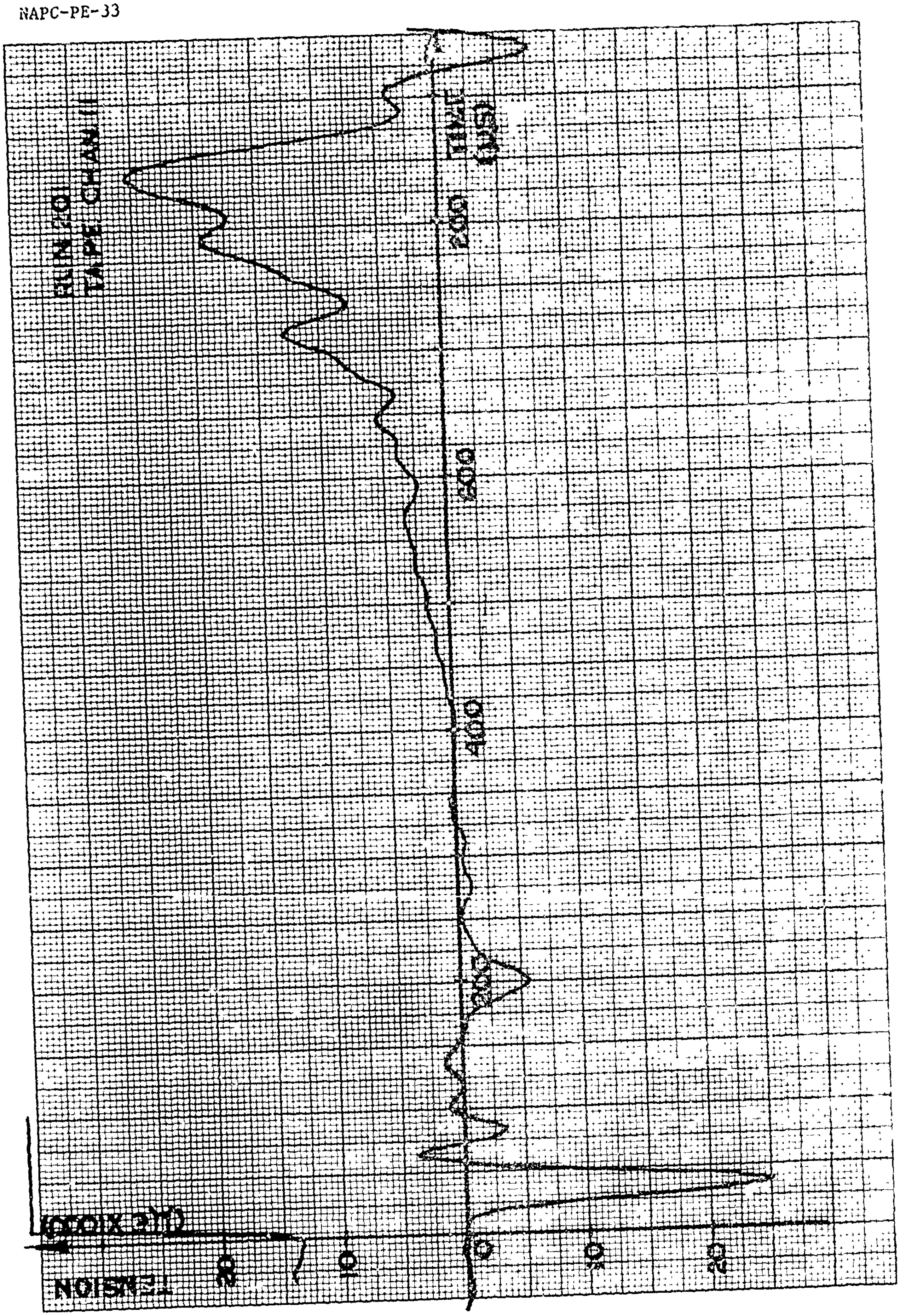

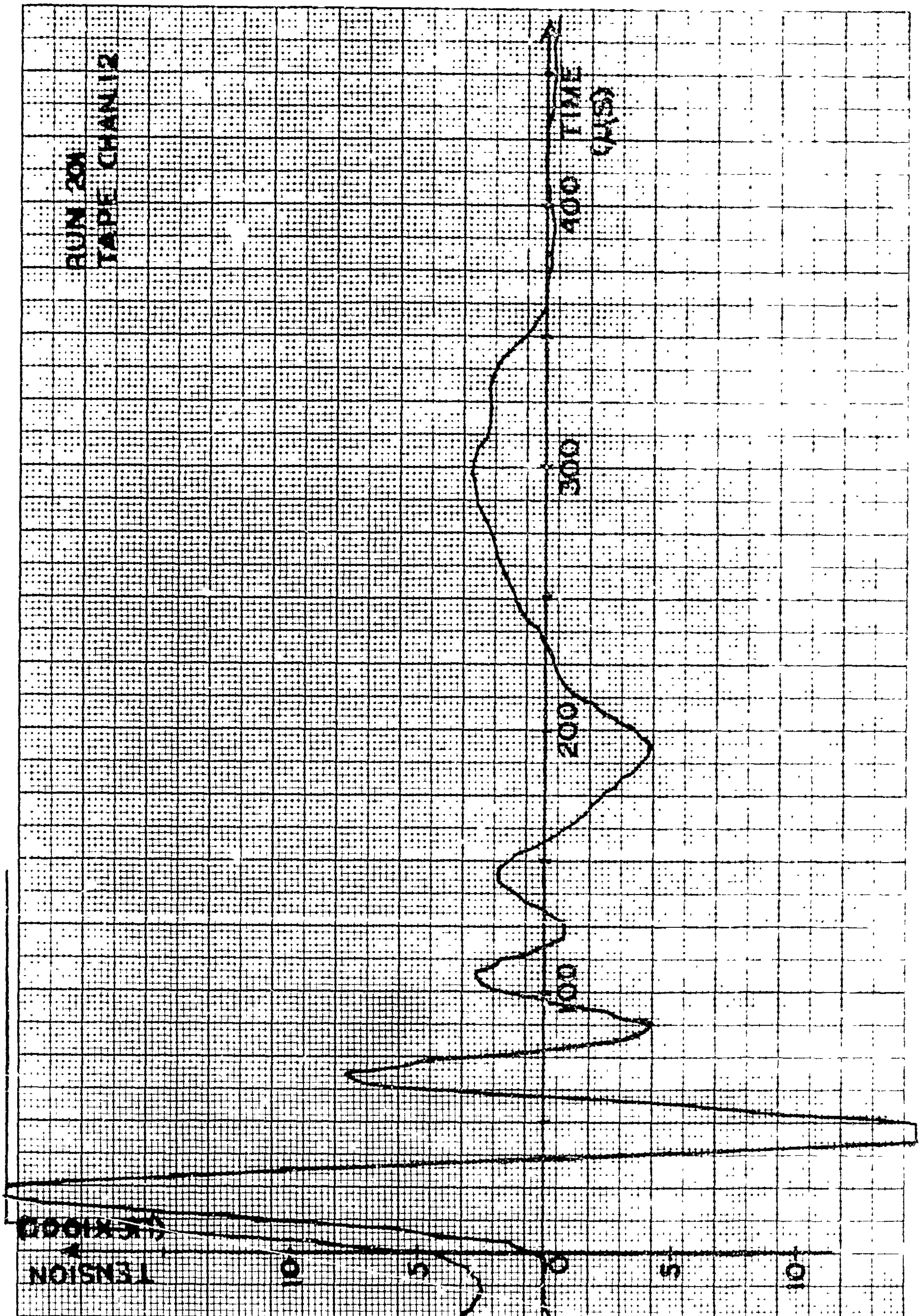
TAPE CHAN 12
TIME
100
200
300
400
TENSION
10
5
0
5
10

DISTRIBUTION LIST

Activity	Copies
Commander, Naval Air Systems Command (AIR-50174), Department of the Navy, Washington, D.C. 20361	9
Intra-command Addresses: AIR-330A (1), AIR-5360 (1), AIR-5362 (1), AIR-530 (1), AIR-5361 (1), MAT-03L (1), AIR-536 (1)	
[illegible]	
Commanding Officer, Naval Air Engineering Center, Lakehurst, NJ 08733	1
Commanding Officer, Naval Aviation Safety Center, Naval Air Station, Norfolk, VA 23511	1
Director, Applied Technology Laboratory, Army Research and Technology Laboratories, Fort Eustis, VA 23604	1
Commanding General, U.S. Army Aviation Systems Command (AMSAV-ERP), 12th and Spruce Streets, St. Louis, MO 63166	1
Commander, Air Force Aeropropulsion Laboratory (AFSC), Wright-Patterson Air Force Base, Dayton, OH 45433	1
National Aeronautics and Space Administration (MS 6-2, MS 49-1, MS 60-3, MS 5-5, MS 3-19, MS 500-302), Lewis Research Center, 21000 Brookpark Road, Cleveland, OH 44135	12
National Aeronautics and Space Administration (RP, RC(2), RLC), Washington, D.C. 20546	4
Federal Aviation Administration (RD-725), Washington, D.C. 20553	1
Defense Documentation Center for Scientific and Technical Information, Building No. 5, Cameron Station, Alexandria, VA 22314	12
Aeroelastic Lab [illegible], Massachusetts Institute of Technology, Cambridge, MA 02139	4